WCAP-11800 SG-88-03-013

BEAVER VALLEY UNIT 1
EVALUATION FOR TUBE
VIBRATION INDUCED FATIGUE

APRIL, 1988

AUTHORS

H.J. CONNORS
T.M. FRICK
J.M. HALL
G.W. HOPKINS
J.L. HOUTMAN
H.M. HU
H.Y. YANT
A.Y. LEE
P.J. PRABHU
R.E. SMITH

APPROVED: T. A. Pitterle

T.A. PITTERLE, MANAGER
STEAM GENERATOR ENGINEERING

WORK PERFORMED UNDER SHOP ORDER DL8D-01304

WESTINGHOUSE ELECTRIC CORPORATION
POWER SYSTEMS BUSINESS UNIT
SERVICE TECHNOLOGY DIVISION
P. O. BOX 3377
PITTSBURGH, PA 15230-0355

ABSTRACT

On July 15, 1987, a steam generator tube rupture event occurred at the North Anna Unit 1 plant. The cause of the tube rupture has been determined to be high cycle fatigue. The source of the loads associated with the fatigue mechanism is a combination of a mean stress level in the tube with a superimposed alternating stress. The mean stress is the result of denting of the tube at the top tube support plate, while the alternating stress is due to out-of-plane deflection of the tube U-bend attributed to flow induced vibration. For tubes without AVB support local flow peaking, effects at unsupported tubes are a significant contribution to tube vibration amplitudes.

This report documents the evaluation of steam generator tubing at Beaver Valley Unit 1 for susceptibility to fatigue-induced cracking of the type experienced at North Anna Unit 1. The evaluation utilizes operating conditions specific to Beaver Valley Unit 1 to account for the plant specific nature of the tube loading and response. The evaluation also includes reviews of eddy current data for Beaver Valley Unit 1 to establish AVB locations. This report provides background of the event which occurred at North Anna, a criteria for fatigue assessment, a summary of test data which support the analytical approach, field measurement results showing AVB positions, thermal hydraulic analysis results, and calculations to determine tube mean stress, stability ratio and tube stress distributions, and accumulated fatigue usage. This evaluation leads to identification of tubes potentially susceptible to fatigue.

SUMMARY OF ABBREVIATIONS

ASME	-	American Society of Mechanical Engineers
ATHOS	-	Analysis of the Thermal Hydraulics of Steam Generators
AVB	-	Anti-Vibration Bar
AVT	-	All Volatile Treatment
ECT	-	Eddy Current Test
EPRI	-	Electric Power Research Institute
FFT	-	Fast Fourier Transform
FLOVIB	-	Flow Induced Vibrations
MEVF	-	Modal Effective Void Fraction
OD	-	Outside Diameter
RMS	-	Root Mean Square
SR	-	Stability Ratio
TSP	-	Tube Support Plate
°F	-	degrees Fahrenheit
hr	-	hour
ksi	-	measure of stress - 1000 pounds per square inch
lb	-	pound
mils	-	0.001 inch
MW	-	mega watt
psi	-	measure of stress - pounds per square inch
psia	-	measure of pressure - absolute

TABLE OF CONTENTS

TABLE OF CONTENTS (CONTINUED)

LIST OF FIGURES

LIST OF FIGURES (Continued)

LIST OF FIGURES (Continued)

LIST OF FIGURES (Continued)

LIST OF TABLES

LIST OF TABLES (Continued)

1.0 INTRODUCTION

This report documents the evaluation of steam generator tubing at Beaver Valley Unit 1 for susceptibility to fatigue-induced cracking of the type experienced at North Anna Unit 1 in July, 1987. The evaluation includes three-dimensional flow analysis of the tube bundle, air-tests performed to support the vibration analytical procedure, field measurements to establish AVB locations, structural and vibration analysis of selected tubes, and fatigue usage calculations to predict cumulative usage for critical tubes. The evaluation utilizes operating conditions specific to Beaver Valley Unit 1 in order to account for plant specific features of the tube loading and response.

Section 2 of the report provides a summary of the Beaver Valley Unit 1 evaluation results and overall conclusions. Section 3 provides background for the tube rupture event which occurred at North Anna Unit 1 including results of the examination of the ruptured tube and a discussion of the rupture mechanism. The criteria for predicting the fatigue usage for tubes having an environment conductive to this type of rupture are discussed in Section 4. Section 5 provides a summary of test data which supports the analytical vibration evaluation of the candidate tubes. A summary of field measurements used to determine AVB locations and ultimately to identify unsupported tubes is provided in Section 6. Section 7 provides the results of a thermal hydraulic analysis to establish flow field characteristics at the top support plate which are subsequently used to assist in identifying tubes which may be dynamically unstable. Section 8 presents an update of the methodology originally used to evaluate the tube rupture at North Anna Unit 1. The final section, Section 9, presents results of the structural and vibration assessment. This section determines tube mean stress, stability ratio and tube stress distributions, and accumulated fatigue usage, forming the basis for the conclusions for Beaver Valley Unit 1.

2.0 SUMMARY AND CONCLUSIONS

The Beaver Valley Unit 1 steam generators are evaluated for the susceptibility of unsupported U-bend tubing with denting at the top tube support plate to a fatigue rupture of the type experienced at Row 9 Column 51 (R9C51) of Steam Generator C, North Anna 1.

2.1 Background

The initiation of the circumferential crack in the tube at the top of the top tube support plate at North Anna 1 has been attributed to limited displacement, fluid elastic instability. The unstable condition prevailed in the R9C51 tube when the tube experienced denting at the support plate. A combination of conditions were present that led to the rupture. The tube is not supported by an anti-vibration bar (AVB), has a higher flow field due to local flow peaking as a result of non-uniform insertion depths of AVB's, has reduced damping because of denting at the top support plate, and has fatigue properties consistent with a lower bound fatigue curve for the material in an all volatile treatment (AVT) water chemistry environment.

2.2 Evaluation Criteria

The criteria established to provide a fatigue usage less than 1.0 for a finite period of time (i.e., 40 years) is a 10% reduction in stability ratio that in turn, would provide a 58% reduction in stress amplitude (to <4.0 ksi) for a Row 9 tube in the North Anna 1 steam generators. This reduction is required to produce a fatigue usage of <0.021 per year for the Row 9 tube. This same criteria is used as one of several criteria in the evaluation of Beaver Valley Unit 1 tubing. With additional effects accounted for through a stress ratio criteria that permits the calculation of fatigue usage to demonstrate tube acceptability, the final criteria of cumulative fatigue usage to date plus future operation with current operating parameters can be satisfied.

The stability ratios for Beaver Valley Unit 1 tubing, the corresponding stress and amplitude, and the resulting cumulative fatigue usage must be evaluated relative to the ruptured tube at Row 9 Column 51, North Anna 1, Steam Generator C, for two reasons. The local effect on the flow field due to

various AVB insertion depths is not within the capability of available analysis techniques and must be determined by test. In addition, an analysis and examination of the ruptured tube at North Anna 1 provided a range of initiating stress amplitudes, but could only bound the possible stability ratios that correspond to these stress amplitudes. Therefore, the evaluation of Beaver Valley Unit 1 tubing has been based on relative stability ratios, relative flow peaking factors, and relative stress ratios.

The criteria for establishing that a tube has support from an AVB and therefore eliminate it from further considerations is that at least [ ]^{a,c} This is established by analysis of eddy current (EC) measurements. AVB support of the tube [ ]^{a,c} may be established by an EC indication of both legs of the AVB or may be established by [ ]^{a,c} the depth of insertion knowing the geometry of the AVB and EC indications that locate it on larger radius tubes.

The AVB insertion depths are a key factor in the assessment of fatigue failure susceptibility since the AVB positions determine the local flow peaking factors. The local flow peaking factor is a direct factor on the apparent stability ratio and a small percentage change causes a significant change in stress amplitude. The relative flow peaking factors for Beaver Valley Unit 1 tubing without direct AVB support have been determined by instability tests. These factors have been applied to relative stability ratios determined by 3-D tube bundle flow analysis and the combined relative stability ratio used in the stress ratio determination.

Eddy current data for the tubes in the area of interest is analyzed to determine the condition of the tubes, and to identify the number and location of tube/AVB interfaces. A more complete explanation of this activity is provided in Section 6 of this report. For the purpose of the tube stability analyses, it was conservatively assumed that all tubes were [ ]^{a,c} (in structural terminology) at the seventh (top) tube support plate (TSP). In fact, eddy current analyses showed that relatively few of the tubes in the area of interest were dented, or showed signs of corrosion at the TSP interface. None of the tubes in the area reviewed showed signs of thinning at AVB interfaces. Therefore, it is unlikely that any of these tubes have been subject to unstable vibration patterns.

In addition to determining the physical condition of the tubes, eddy current data was used to determine AVB insertions depths, and the extent of AVB support for each column of tubes in the area of interest. Review of the eddy current data shows that only in the center 1/3 of the tube bundle were the tubes not supported as far in as row eight or row nine. Within the three SG's, support could not be verified for one row 12 tube, 6 row 11 tubes, and 23 row 10 tubes.

Fifteen tubes are identified as the more susceptible of the unsupported tubes. All of these tubes have been evaluated as dented. These are:

S/G	TUBE	S/G	TUBE	S/G	TUBE
A	R9C35	B	R9C35	C	R9C60
	R9C47		R9C47		R10C47
	R10C43		R9C60		R10C60
	R10C47				R11C47
	R11C49				R11C51
					R11C52
					R12C51

The local flow peaking corresponding to AVB insertion depths are factored into the evaluation for each of the above tubes. This results in the relative stability ratios and stress ratios shown below. (All ratios are in comparison to R9C51, North Anna Unit 1, Steam Generator C.)

Generator	Tube	Stability Ratio	Stress
A	R9C35	0.73	0.31
	R9C47	0.66	0.18
	R10C43	0.89	0.81
	R10C47	0.77	0.35
	R11C49	0.88	0.64
B	R9C47	0.66	0.18
	R9C60	0.86	0.77
	R9C35	0.86	0.77

Generator	Tube	Stability Ratio	Stress
C	R9C60	0.86	0.77
	R10C47	0.77	0.35
	R10C60	1.081	>>1.0
	R11C47	1.272	>>1.0
	R11C51	1.454	>>1.0
	R11C52	1.454	>>1.0
	R12C51	>1.12	>>1.0

With the exception of five tubes in Steam Generator C all tubes have relative stability ratios (including flow pe[illegible] less than 0.9 and stress ratios less than 1.0. The five tubes exceeding [illegible] criteria are R12C51, R11C52, R11C51, R11C47, and R10C60 in Steam Generator C. Six tubes have been plugged as a preventive measure to eliminate them from further consideration. Sentinel, or tell-tale, plugs were used to permit detection of tube degradation if it should occur in the future. One tube R10C43, was plugged in Steam Generator A, based on preliminary analytical results. Final analysis indicates plugging of that tube was not necessary.

Of the remaining tubes that meet the criterion, the tubes at R9C35 and R9C60 have the highest stress ratio 0.77. The expected maximum stress amplitude for this tube is 3.1 ksi. Based on the operating history of Beaver Valley 1, which is presented in Figure 7-15 (see Section 7) in the form of normalized stability ratio versus time in days, the fatigue usage for 40 years is expected to be less than 0.346. This is less than the ASME Code limit of 1.0. The fatigue usage calculation utilizes a lower bound fatigue curve that is consistent with the fatigue properties of the North Anna tube that ruptured.

2.3 Conclusion

The Beaver Valley 1 tubes remaining in service are not expected to be susceptible to fatigue rupture at the top support plate in a manner similar to the rupture which occurred at North Anna 1. Therefore, no modification, preventive tube plugging, or other measure to preclude such an event is judged to be necessary other than the plugging of the five tubes in Steam Generator C. The one tube in Steam Generator A, R10C43, may be returned to service during a future outage.

3.0 BACKGROUND

On July 15, 1987, a steam generator tube rupture occurred at the North Anna Unit 1. The ruptured tube was determined to be Row 9 Column 51 in steam generator "C". The location of the opening was found to be at the top tube support plate on the cold leg side of the tube and was circumferential in orientation with a 360 degree extent.

3.1 North Anna Unit 1 Tube Rupture Event

The cause of the tube rupture has been determined to be high cycle fatigue. The source of the loads associated with the fatigue mechanism has been determined to be a combination of a mean stress level in the tube and a superimposed alternating stress. The mean stress has been determined to have been increased to a maximum level as the result of denting of the tube at the top tube support plate and the alternating stress has been determined to be due to out-of-plane deflection of the tube U-bend above the top tube support caused by flow induced vibration. These loads are consistent with a lower bound fatigue curve for the tube material in an AVT water chemistry environment. The vibration mechanism has been determined to be fluid elastic, based on the magnitude of the alternating stress.

A significant contributor to the occurrence of excessive vibration is the reduction in damping at the tube-to-tube support plate interface caused by the denting. Also, the absence of antivibration bar (AVB) support has been concluded to be required for requisite vibration to occur. The presence of an AVB support restricts tube motion and thus precludes the deflection amplitude required for fatigue. Inspection data shows that an AVB is not present for the Row 9 Column 51 tube but that the actual AVB installation depth exceeded the minimum requirements in all cases with data for AVBs at many other Row 9 tubes. Also contributing significantly to the level of vibration, and thus loading, is the local flow field associated with the detailed geometry of the steam generator, i.e., AVB insertion depths. In addition, the fatigue properties of the tube reflect the lower range of properties expected for an

AVT environment. In summary, the prerequisite conditions derived from the evaluations were concluded to be:

Fatigue Requirements	Prerequisite Conditions
Alternating stress	Tube vibration - Dented support - Flow excitation - Absence of AVB
Mean stress	Denting in addition to applied stress
Material fatigue properties	AVT environment - Lower range of properties

3.2 Tube Examination Results

Fatigue was found to have initiated on the cold leg outside surface of Tube R9C51 immediately above the top tube support plate. No indications of significant accompanying intergranular corrosion was observed on the fracture face or on the immediately adjacent OD surfaces. Multiple fatigue initiation sites were found with major sites located at 110°, 120°, 135° and 150°, Figure 3-1. The plane of the U-bend is located at 45° with the orientation system used, or approximately 90° from the geometric center of the initiation zone at Section D-D. High cycle fatigue striation spacings approached 1 micro-inch near the origin sites, Figure 3-2. The early crack front is believed to have broken through-wall from approximately 100° to 140°. From this point on, crack growth is believed (as determined by striation spacing, striation direction, and later observations of parabolic dimples followed by equiaxed dimples) to have accelerated and to have changed direction with the resulting crack front running perpendicular to the circumferential direction.

3.3 Mechanism Assessment

To address a fatigue mechanism and to identify the cause of the loading, any loading condition that would cause cyclic stress or steady mean stress had to be considered. The analysis of Normal, Upset and Test conditions indicated a relatively low total number of cycles involved and a corresponding low fatigue usage, even when accounting for the dented tube condition at the plate. This analysis also showed an axial tensile stress contribution at the tube OD a short distance above the plate from operating pressure and temperature, thus providing a contribution to mean stress. Combining these effects with denting deflection on the tube demonstrated a high mean stress at the failure location. Vibration analysis for the tube developed the characteristics of first mode, cantilever response of the dented tube to flow induced vibration for the uncracked tube and for the tube with an increasing crack angle, beginning at 90° to the plane of the tube and progressing around on both sides to complete separation of the tube.

Crack propagation analysis matched cyclic deformation with the stress intensities and striation spacings indicated by the fracture inspection and analysis. Leakage data and crack opening analysis provided the relationship between leak rate and circumferential crack length. Leakage versus time was then predicted from the crack growth analysis and the leakage analysis with initial stress amplitudes of 5, 7, and 9ksi. The comparison to the best estimate of plant leakage (performed after the event) showed good agreement, Figure 3-3.

Based on these results, it followed that the predominant loading mechanism responsible is a flow-induced, tube vibration loading mechanism. It was shown that of the two possible flow-induced vibration mechanisms, turbulence and fluidelastic instability, that fluidelastic instability was the most probable cause. Due to the range of expected initiation stress amplitudes (4 to 10ksi), the fluidelastic instability would be limited in displacement to a range of approximately [ ]^{a,c} This is less than the distance between tubes at the apex, [ ]^{a,c} It was further confirmed that displacement prior to the rupture was limited since no indication of tube U-bend (apex region) damage was evident in the eddy-current signals for adjacent tubes.

Given the likelihood of limited displacement, fluidelastic instability, a means of establishing the change in displacement, and corresponding change in stress amplitude, was developed for a given reduction in stability ratio (SR). Since the rupture was a fatigue mechanism, the change in stress amplitude resulting from a reduction in stability ratio was converted to a fatigue usage benefit through the use of the fatigue curve developed. Mean stress effects were included due to the presence of denting and applied loadings. The results indicated that a 10% reduction in stability ratio is needed (considering the range of possible initiation stress amplitudes) to reduce the fatigue usage per year to less than 0.02 for a tube similar to Row 9 Column 51 at North Anna Unit 1.

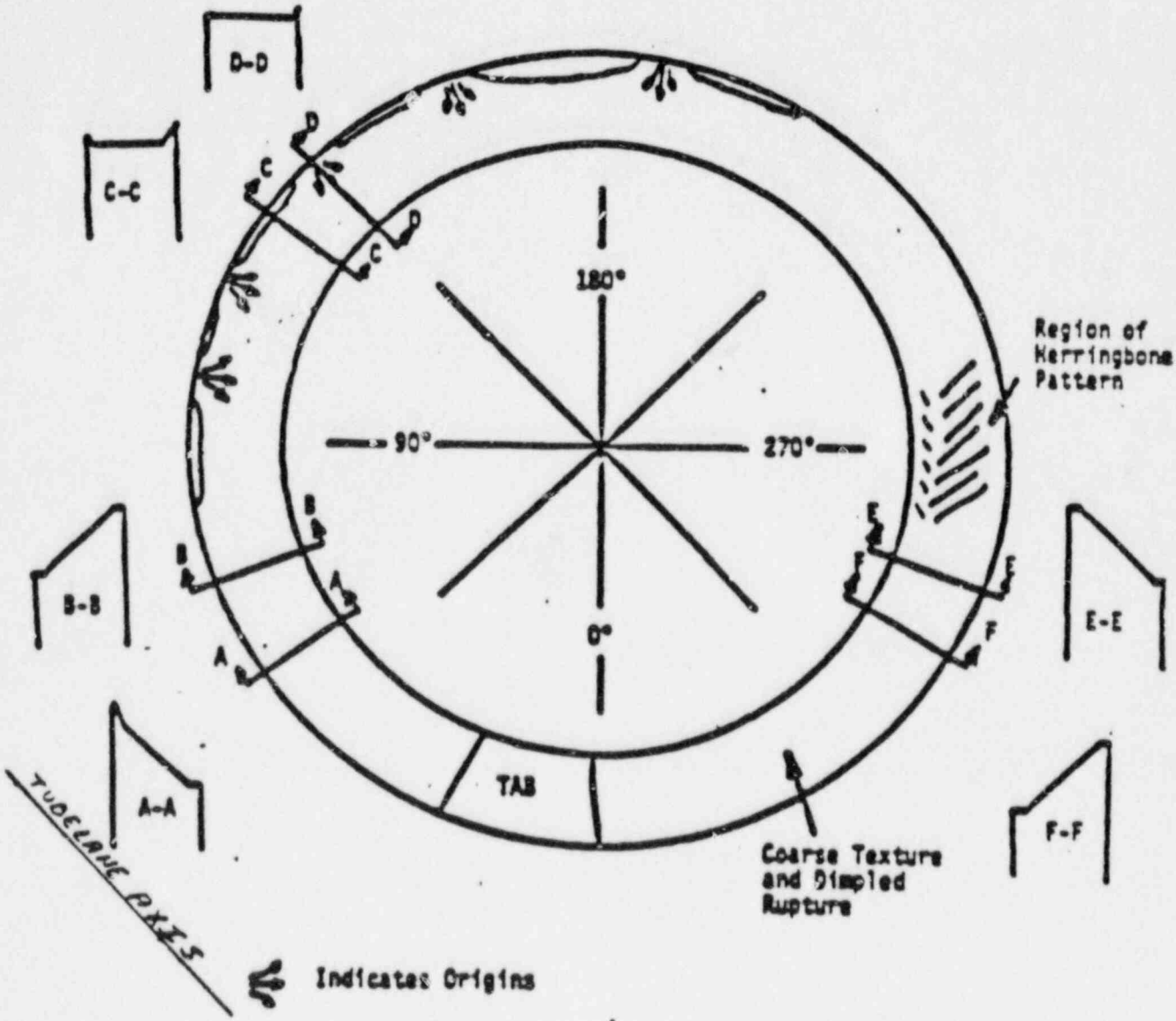

Figure 3-1 Approximate Mapping of Fracture Surface of Tube R9C51, S/G "C" Cold Leg, North Anna Unit 1

0144M:49/030788-21

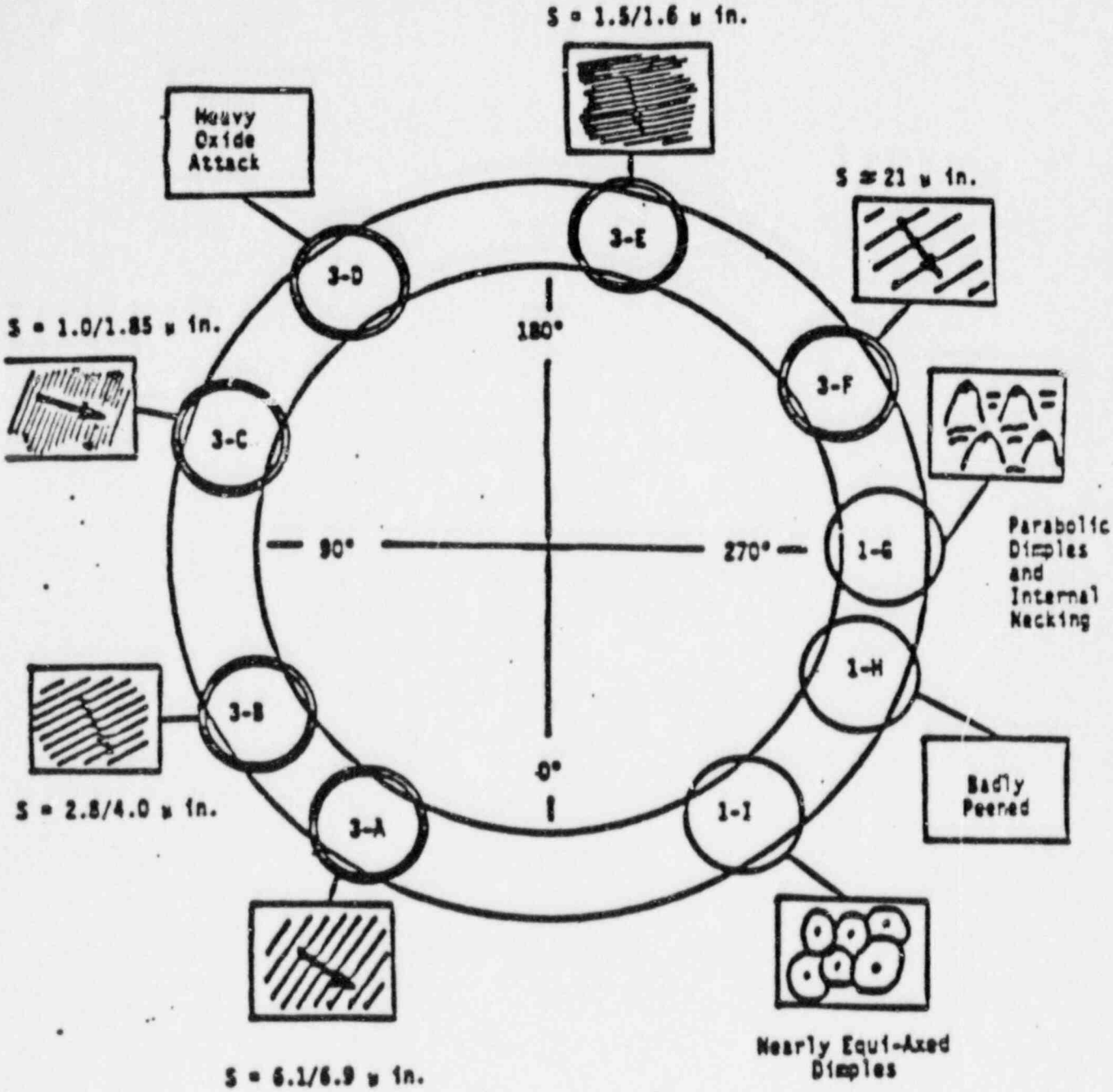

Note: Arrows Indicate Direction of Fracture Propagation

Figure 3-2 Schematic Representation of Features Observed During TEM Fractograhic Examination of Fracture Surface of Tube R9C51, S/G "C" Cold Leg, North Anna Unit 1

0144M:49/030788-22

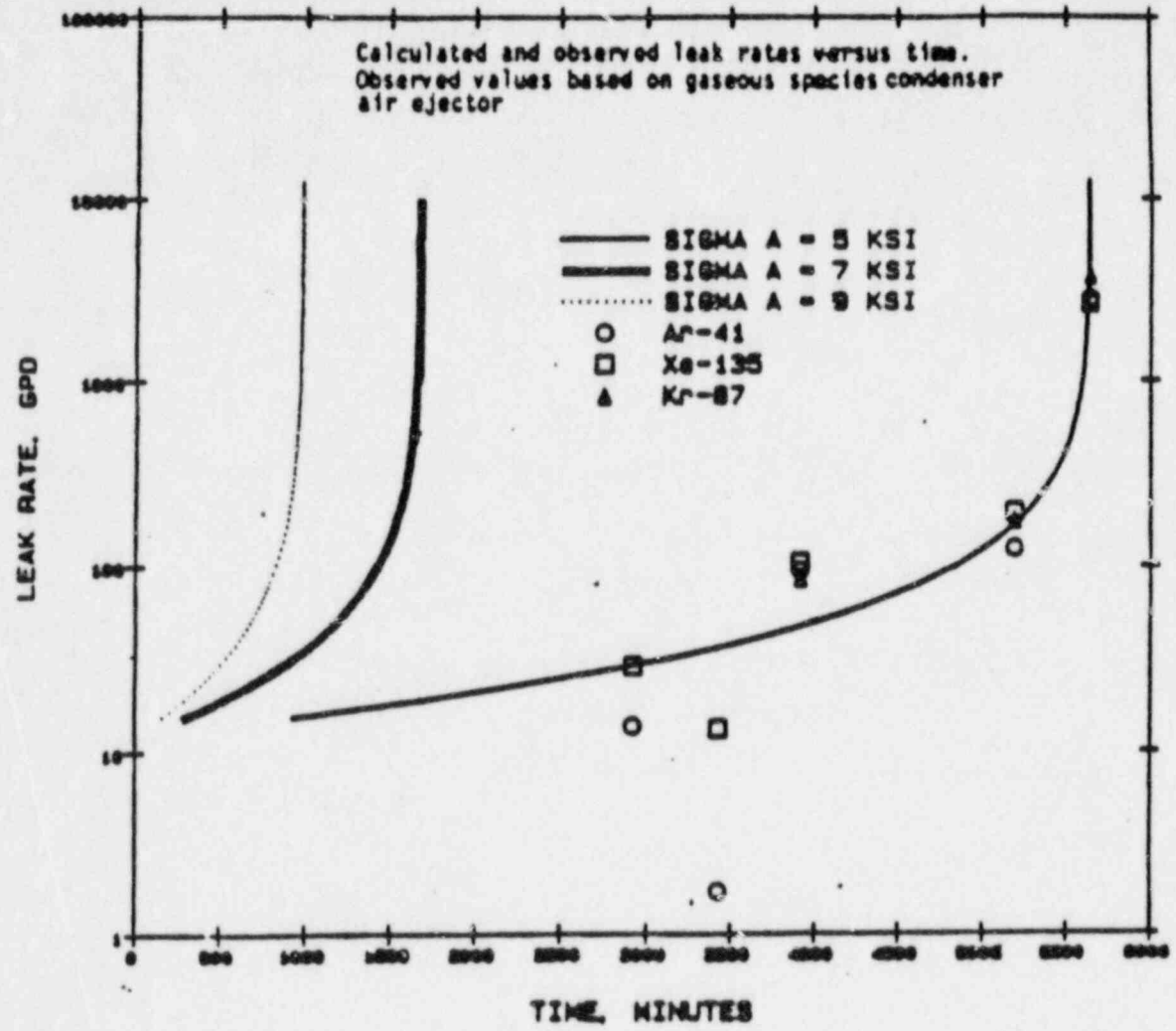

Figure 3-3 Calculated and Observed Leak Rates Versus Time

4.0 CRITERIA FOR FATIGUE ASSESSMENT

Evaluation against criteria to show that Beaver Valley Unit 1 steam generator tubing will not rupture by fatigue in the manner of North Anna Unit 1 can only be done by an assessment relative to the Row 9 Column 51 tube of Steam Generator C, North Anna Unit 1, since, 1) methods for direct analytical prediction of actual stability ratios incorporate greater uncertainties than a relative ratio, and 2) the stress amplitude (or displacement) associated with a specific value of stability ratio can only be estimated by the analysis of North Anna Unit 1. For these reasons, the North Anna Unit 1 tubing evaluation was done on a relative basis to Row 9 Column 51 and a 10% reduction in stability ratio criteria was established to demonstrate that tubes left in service would be expected to have sufficiently low vibration stress to preclude future fatigue rupture events.

To accomplish the necessary relative assessment of Beaver Valley Unit 1 tubing to Row 9 Column 51 of North Anna Unit 1, several criteria are utilized. First, stability ratios are calculated for Beaver Valley Unit 1 steam generators based on flow fields predicted by 3-D thermal hydraulic models and ratioed to the stability ratio for Row 9 Column 51 at North Anna Unit 1 based on a flow field obtained with a 3-D thermal hydraulic model with the same degree of refinement. These ratios of stability ratio (called relative stability ratios) for each potentially unsupported U-bend in the Beaver Valley Unit 1 steam generators should be equivalent to ≤ 0.9 of R9C51, North Anna 1 (meeting the 10% reduction in stability ratio criteria). This provides the first level of screening of susceptible tubes incorporating all tube geometry and flow field differences in the tube dynamic evaluation. It has the inherent assumption, however, that each tube has[

]^{a,c} To account for these differences, flow peaking factors can be incorporated in the relative stability ratios or, as noted below, in the relative stress ratios.

The second criteria is to obtain stress ratios, the ratio of stress in the Beaver Valley Unit 1 tube of interest to the stress in Row 9 Column 51, North Anna Unit 1, and, after incorporating the requirement that the relative stability ratio to Row 9 Column 51 (R9C51) for the tube of interest is equivalent to ≤ 0.9, require the stress ratio to be ≤ 1.0. The stress ratio incorporates the [ ]^{a,c} with R9C51 in relation to the stress calculation and also incorporates the ratio of flow peaking factor for the Beaver Valley Unit 1 tube of interest to the flow peaking factor for R9C51 (flow peaking factor is defined in Section 4.2). This should provide that all tubes meeting this criteria have stress amplitudes ≤ 4.0 ksi.

Finally, the cumulative fatigue usage for plant operation to date and for continued operation with the same operating parameters is evaluated. A fatigue usage of ≤ 1.0 is not necessarily satisfied by meeting the stress ratio criteria since the evaluation for Beaver Valley Unit 1 has been performed for a reference operating cycle. The Beaver Valley Unit 1 duty cycle was more demanding in early cycles and usage would have accumulated at a more rapid rate. Therefore, the time history of operation is evaluated on a normalized basis and used together with the stress ratio to obtain a stress amplitude history. This permits the calculation of current and future fatigue usage for comparison to 1.0.

4.1 Stability Ratio Reduction Criteria

For fluidelastic evaluation, stability ratios are determined for specific configurations of a tube. These stability ratios represent a measure of the potential for flow-induced tube vibration during service. Values greater than unity (1.0) indicate instability (see Section 5.1).

Motions developed by a tube in the fluidelastically unstable mode are quite large in comparison to the other known mechanisms. The maximum modal displacement (at the apex of the tube) is linearly related to the bending stress in the tube just above the cold leg top tube support plate. This relationship applies to any vibration in that mode. Thus, it is possible for an unstable, [ ]^{a,c} boundary condition tube to deflect an amount in the U-bend which will produce fatigue inducing stresses.

The major features of the fluidelastic mechanism are illustrated in Figure 4-1. This figure shows the displacement response (LOG D) of a tube as a function of stability ratio (LOG SR). A straight-line plot displayed on log-log coordinates implies a relation of the form $y = A(x)^n$, where A is a constant, x is the independent variable, n is the exponent (or power to which x is raised), and y is the dependent variable. Taking logs of both sides of this equation leads to the slope-intercept form of a straight-line equation in log form, $\log y = c + n \log x$, where $c = \log A$ and represents the intercept and n is the slope. In our case the independent variable x is the stability ratio SR, and the dependent variable y is tube (fluidelastic instability induced) displacement response D, and the slope n is renamed s.

From experimental results, it is known that the turbulence response curve (on log-log coordinates) has a slope of approximately [ ]^{a,b,c} Test results also show that the slope for the fluidelastic response depends somewhat on the instability displacement (response amplitude). It has been shown by tests that a slope of [ ]^{a,b,c} is a range of values corresponding to displacement amplitudes in the range of [ ]^{a,c} whereas below [ ]^{a,c} are conservative values.

The reduction in response obtained from a stability ratio reduction can be expressed by the following equation:

[ ]^{a,c}

where D_1 and SR_1 are the known values at the point corresponding to point 1 of Figure 4-1 and D_2 and SR_2 are values corresponding to any point lower on this curve. Therefore, this equation can be used to determine the reduction in displacement response for any given reduction in stability ratio.

This equation shows that there is benefit derived from even a very small percentage change in the stability ratio. It is this reduction in displacement for a quite small reduction in stability ratio that formed the basis for demonstrating that a 10% reduction in stability ratio would be sufficient to prevent Row 9 Column 51 from rupturing by fatigue.

The fatigue curve developed for the North Anna Unit 1 tube at R9C51 is from [

] a,c Thus,

[ ] a,c

where, σ_a is the equivalent stress amplitude to σ_a that accounts for a maximum stress of σ_y, the yield strength. The -3 sigma curve with mean stress effects is shown in Figure 4-2 and is compared to the ASME Code Design Fatigue Curve for Inconel 600 with the maximum effect of mean stress. The curve utilized in this evaluation is clearly well below the code curve reflecting the effect of an AVT environment on fatigue and [ ] a,c for accounting for mean stress that applies to materials in a corrosive environment.

Two other mean stress models were investigated for the appropriateness of their use in providing a reasonable agreement with the expected range of initiating stress amplitudes. These were the [ ] a,c shown in Figure 4-3. With a [ ] a,c the [

] a,c

] a,c.

The assessment of the benefit of a reduction in stability ratio begins with the relationship between stability ratio and deflection. For a specific tube geometry, the displacement change is directly proportional to change in stress so that stress has the same relationship with stability ratio,

$$[\quad]^{a,c}$$

The slope in this equation can range from $[\quad]^{a,c}$ on a log scale depending on the amplitude of displacement. Knowing the stress resulting from a change in stability ratio from SR_1 to SR_2, the cycles to failure at the stress amplitude was obtained from the fatigue curve. A fatigue usage per year was then determined assuming continuous cycling at the natural frequency of the tube. The initial stress was determined to be in the range of 4.0 to 10.0 ksi by the fractography analysis.

It was further developed that the maximum initiating stress amplitude was not more than 9.5 ksi. This was based on [

$]^{a,c}$ The corresponding stress level is 5.6 ksi.

The maximum stress, 9.5 ksi, would be reduced to $[\quad]^{a,c}$ with a 10% reduction in stability ratio and would have a future fatigue usage of $[\quad]^{a,c}$ per year at 75% availability, Figure 4-4. The minimum stress, 5.6 ksi, would be reduced to $[\quad]^{a,c}$ with a 5% reduction in stability ratio and would have future fatigue usage of $[\quad]^{a,c}$ per year, Figure 4-5. In addition, if a tube were already cracked, it could be as large as $[\quad]^{a,c}$ inch in length and thru-wall and would not propagate if the stress amplitudes are reduced to $\leq$ 4.0 ksi.

Subsequent to the return to power evaluation for North Anna Unit 1, the time history of operation was evaluated on a normalized basis to the last cycle. [

]a,c cumulative fatigue usage may then be computed to get a magnitude of alternating stress for the last cycle that results in a cumulative usage of 1.0 for the nine-year duty cycle. The result of the iterative analysis is that the probable stress associated with this fatigue curve during the last cycle of operation was approximately [ ]a,c for R9C51, North Anna Unit 1, Steam Generator C, and that the major portion of the fatigue usage came in the second, third and fourth cycles. The first cycle was conservatively omitted, since denting is assumed, for purposes of this analysis, to have occurred during that first cycle. Based on this evaluation, the tube fatigue probably occurred over most of the operating history of North Anna Unit 1.

A similar calculation can be performed for the time history of operation assuming that [

]a,c On this basis, the effect of a 10% reduction in stability ratio is to reduce the stress amplitude to 4.0 ksi and results in a future fatigue usage of [ ]a,c

Other combinations of alternating stress and mean stress were evaluated with -3 sigma and -2 sigma fatigue curves to demonstrate the conservatism of the 10% reduction in stability ratio. Table 4-1 presents the results of the cases analyzed clearly demonstrating that the 10% reduction in stability ratio combined with a -3 sigma fatigue curve and with maximum mean stress effects is conservative. Any higher fatigue curve whether through mean stress, mean stress model, or probability, results in greater benefit for the same reduction in stability ratio. Further, for any of these higher curves, a smaller reduction in stability ratio than 10% would result in the same benefit. In addition, there is a large benefit in terms of fatigue usage for relatively small changes in the fatigue curve.

4.2 Local Flow Peaking Considerations

Local flow peaking is a factor on stability ratio that incorporates the effect on [ ]^{a,c} due to non-uniform AVB insertion depths. The flow peaking factor is applied directly to the stability ratio obtained from thermal-hydraulic analysis that does not account for these local geometry effects. Being a direct factor on stability ratio, a small percentage increase can result in a significant change in the prediction of tube response.

Since the evaluation of Beaver Valley Unit 1 is relative to R9C51, North Anna Unit 1, the flow peaking factors are also applied as relative ratios, i.e., a ratio of Beaver Valley Unit 1 to R9C51 at North Anna Unit 1. The flow peaking relative instability is obtained by testing in the air test rig described in Section 5.4, where the peaking factor is defined as the critical velocity for R9C51 AVB pattern compared to critical velocity for a uniform AVB pattern. As explained in Section 8.0, the minimum value of [ ]^{a,b,c} is appropriate for R9C51 of North Anna 1. The peaking factor for a tube in Beaver Valley Unit 1 is therefore divided by [ ]^{a,b,c} and the resulting relative flow peaking is multiplied times the relative stability ratio based on ATHOS results. If the peaking factor is 1.0, the relative flow peaking is [ ]^{a,b,c}

Applying a nominal uncertainty of 15% to the ATHOS analysis result, the predicted stability ratio for R9C51 is [ ]^{a,b,c} using nominal damping that is a function of the modal effective void fraction (slip). Applying the [ ]^{a,b,c} factor gives a corrected stability ratio of [ ]^{a,b,c}. Therefore, using the minimum flow peaking factor and nominal damping that reflects reduced damping compared to undented tubes, the tube at R9C51, North Anna Unit 1, Steam Generator C is shown to be unstable by comparison to the same tube with a uniform AVB pattern. It is therefore now considered to be sufficient to address the relative susceptibility of tubes to fatigue rupture on [

]^{a,c}

4.3 Stress Ratio Considerations

In Section 4.1, a 10% reduction in stability ratio was established to reduce the stress amplitude on the Row 9 Column 51 tube of North Anna Unit 1 to a level that would not have ruptured, 4.0 ksi. To apply this same criteria to another tube in the same or another steam generator, the differences in [

]a,c

[

]a,c

[

]a,c

By establishing their equivalent effect on the stress amplitude that produced the tube rupture at North Anna 1, several other effects may be accounted for. These include a lower mean stress (such as for non-dented tubes), different frequency tubes from the [ ]a,c,e hertz frequency of R9C51, North Anna 1, and shorter design basis service (such as 30 years).

In the case of lower mean stress, the stress amplitude that would have caused the failure of R9C51, North Anna 1, would have been higher. [

]a,c

A lower or higher frequency tube would not reach a usage of 1.0 in the same length of time as the R9C51 tube due to the different frequency of cycling. The usage accumulated is proportional to the frequency and, therefore, the allowable number of cycles to reach a usage of 1.0 is inversely proportional to frequency. The equivalent number of cycles to give the usage of 1.0 for a different frequency tube [

]a,c

For a different time basis for fatigue usage evaluation, [

]a,c,e

Knowing the magnitude of the stress ratio allows 1) the determination of tubes that do not meet a value of ≤ 1, and 2) the calculation of maximum stress in the acceptable tubes,

[ ]a,c

Having this maximum stress permits the evaluation of the maximum fatigue usage for Beaver Valley Unit 1 based on the time history expressed by normalized stability ratios for the duty cycle (see Section 7.4).

Table 4-1

Fatigue Usage per Year Resulting

From Stability Ratio Reduction

SR, % REDUCTION	STRESS BASIS(1)	FATIGUE CURVE(2)	MEAN STRESS MODEL	USAGE PER YEAR
5.	9 yrs to fail (5.6)	[	]a,c	0.0207
5.	9 yrs to fail (7.0)			0.0107
5.	9 yrs to fail (8.0)			0.0014
10.	max. stress amplitude(4) (9.5)			0.0209
10.	max. stress amplitude(4) (9.5)			0.0053
10.	max. stress amplitude(4) (10.3)			0.0004
10.	max. stress amplitude(4) (11.6)			0.0142
10.	max. stress based on duty cycle(5) (9.5)	]		0.0020

(1) This gives the basis for selection of the initiating stress amplitude and its value in ksi.

(2) S_m is the maximum stress applied with $S_m = S_{mean} + S_a$.

(3) [ ]a,c

(4) Cycles to failure implied by this combination of stress and fatigue properties is notably less than implied by the operating history. Consequently this combination is a conservative, bounding estimate.

(5) Cycles to failure implied by the operating history requires 1.3 sigma fatigue curve at the maximum stress of 9.5 ksi.

[

]a,b,c

Figure 4-1 Vibration Displacement vs. Stability Ratio

[ ] a,c

Figure 4-2 Fatigue Strength of Inconel 600 in AVT Water at 600°F

[ ] a,c

Figure 4-3 Fatigue Curve for Inconel 600 in AVT Water
Comparison of Mean Stress Correction Models

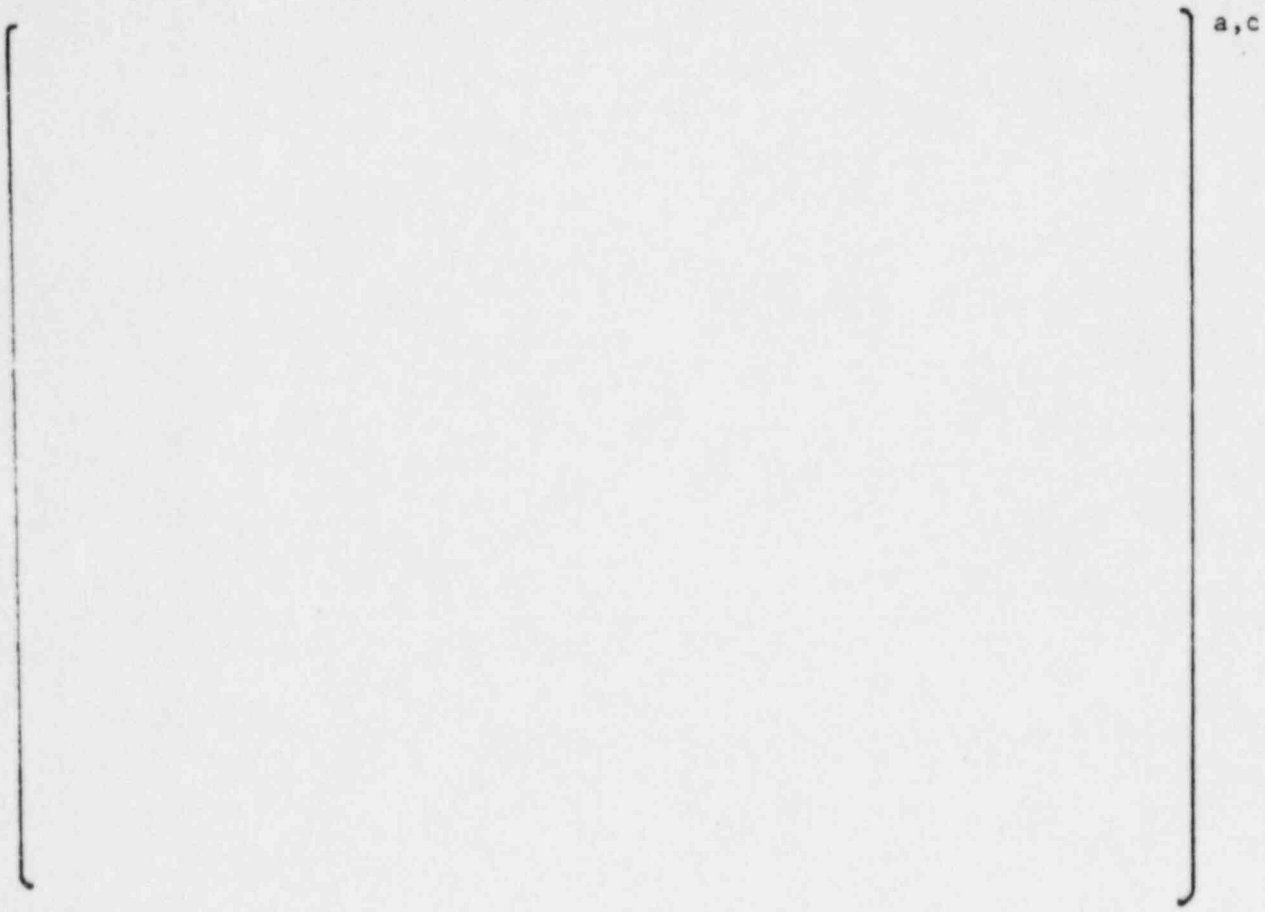

Figure 4-4 Modified Fatigue with 10% Reduction in Stability Ratio for Maximum Stress Condition

Figure 4-5 Modified Fatigue with 5% Reduction in Stability Ratio for Minimum Stress Condition

5.0 SUPPORTING TEST DATA

This section provides a mathematical description of the fluid-elastic mechanism, which was determined to be the most likely causative mechanism for the North Anna tube rupture, as discussed in Section 3.3, to highlight the physical conditions and corresponding parameters directly related to the event and associated preventative measures. The basis for establishing the appropriate values and implications associated with these parameters are provided. Where appropriate, test results are presented.

5.1 Stability Ratio Parameters

Fluid-elastic stability ratios are obtained by evaluations for specific configurations, in terms of active tube supports, of a specific tube. These stability ratios represent a measure of the potential for tube vibration due to instability during service. Fluid-elastic stability evaluations are performed with a computer program which provides for the generation of a finite element model of the tube and tube support system. The finite element model provides the vehicle to define the mass and stiffness matrices for the tube and its support system. This information is used to determine the modal frequencies (eigenvalues) and mode shapes (eigenvectors) for the linearly supported tube being considered.

The methodology is comprised of the evaluation of the following equations:

Fluid-elastic stability ratio = SR = U_{en}/U_c for mode n,

where U_c (critical velocity) and U_{en} (effective velocity) are determined by:

$$U_c = \beta\, f_n\, D\, ((m_o\, \delta_n) / (\rho_o\, D^2))^{1/2} \qquad [1]$$

and;

$$U_{en}^2 = \frac{\sum_{j=1}^{N} (\rho_j/\rho_o)\, U_j^2 \phi_{jn}^2\, z_j}{\sum_{j=1}^{N} (m_j/m_o)\, \phi_{jn}^2\, z_j} \qquad [2]$$

where,

D = tube outside diameter, inches

U_{en} = effective velocity for mode n, inches/sec

N = number of nodal points of the finite element model

m_j, U_j, ρ_j = mass per unit length, crossflow velocity and fluid density at node j, respectively

ρ_o, m_o = reference density and a reference mass per unit length, respectively (any representative values)

δ_n = logarithmic decrement (damping)

ϕ_{jn} = normalized displacement at node j in the nth mode of vibration

z_j = average of distances between node j to j-1, and j to J+1

β = an experimentally correlated stability constant

Substitution of Equations [1] and [2] into the expression which defines stability ratio, and cancellation of like terms, leads to an expression in fundamental terms (without the arbitrary reference mass and density parameters). From this resulting expression, it is seen that the stability ratio is directly related to the flow field in terms of the secondary fluid velocity times square-root-density distribution (over the tube mode shape), and inversely related to the square root of the mass distribution, square root of modal damping, tube modal frequency, and the stability constant (beta).

The uncertainty in each of these parameters is addressed in a conceptual manner in Figure 5-1. The remainder of this section (Section 5.0) provides a discussion, and, where appropriate, the experimental bases to quantitatively establish the uncertainty associated with each of these parameters. In

addition, Section 5.3 provides the experimental basis to demonstrate that tubes with [ ]^{a,c} This implies that those tubes with [ ]^{a,c} would not have to be modified because their instability response amplitude (and stress) would be small. The very high degree of sensitivity of tube response (displacements and stresses) to changes in the velocity times square-root-density distribution is addressed in Section 4.0. This is important in determining the degree of change that can be attained through modifications.

Frequency

It has been demonstrated by investigators that analytically determined frequencies are quite close to their physical counterparts obtained from measurements on real structures. Thus, the uncertainty in frequencies has been shown to be quite small. This is particularly appropriate in the case of dented [ ]^{a,c} tubes. Therefore, uncertainty levels introduced by the frequency parameter are expected to be insignificant (see also "Average Flow Field" subsection below).

Instability Constant (Beta)

The beta (stability constant) values used for stability ratio and critical velocity evaluations (see above equations) are based on an extensive data base comprised of both Westinghouse and other experimental results. In addition, previous field experiences are considered. Values have been measured for full length U-bend tubes in prototypical steam/water environments. In addition, measurements in U-bend air models have been made with both no AVB and variable AVB supports (Figure 5-3).

To help establish the uncertainties associated with ATHOS flow velocity and density distribution predictions on stability analyses, the Model Boiler (MB-3) tests performed at Mitsubishi Heavy Industries (MHI) in Japan were modeled using ATHOS. A beta value consistent with the ATHOS predicted flow conditions and the MB-3 measured critical velocity was determined. These analyses supported a beta value of [ ]^{a,b,c}

A summary of the test bases and qualifications of the beta values used for these assessments is provided by Figure 5-2. The lowest measured beta for tubes without AVBs was a value of [ ]^{a,b,c} This value is used for the beta parameter in all stability ratio evaluations addressed in this Report (see also "Average Flow Field" subsection below).

Mass Distribution

The mass distribution parameter is based on known information on the tube and primary and secondary fluid physical properties. The total mass per unit length is comprised of that due to the tube, the internal (primary) fluid, and the external (secondary) fluid (hydrodynamic mass). Data in Reference 5-2 suggests that at operating void fractions the [

]^{a,c}

Tube Damping

Test data are available to define tube damping for [ ]^{a,c} tube supports, appropriate to dented tube conditions, in steam/water flow conditions. Prototypic U-bend testing has been performed under conditions leading to [ ]^{a,c} supports. The data of [ ]^{a,c} in Figure 5-4 provides the principal data for [ ]^{a,c} tube conditions in steam/water. This data was obtained for cross flow over straight tubes. Uncertainties are not defined for the data from these tests. Detailed tube damping data used in support of the stability ratio evaluations addressed in this report are provided in Section 5.2, below.

Flow Field - Velocity Times Square-Root-Density Distribution

Average and U-bend-local flow field uncertainties are addressed independently in the following.

Average Flow Field

Uncertainties in the average flow field parameters, obtained from ATHOS analyses, coupled with stability constant and frequency, are essentially the same for units with dented or non-dented top support plates. If the errors associated with these uncertainties were large, similar instabilities would be expected in the non-dented units with resulting wear at either the top support plate or inner row AVBs. Significant tube wear has not been observed in inner row tubes in operating steam generators without denting. Thus, an uncertainty estimate of about [ ]^{a,c} for the combined effects of average flow field, stability constant and frequency appears to be reasonable. To further minimize the impact of these uncertainties, the Beaver Valley Unit 1 tubes are evaluated on [ ]^{a,c} Thus, the uncertainties associated with the average velocity times square-root-density (combined) parameter are not expected to be significant.

U-Bend Local Flow Field

Non-uniform AVB insertion depths have been shown to have effects on stability ratios. Flow peaking, brought about by the "channeling" effects of non-uniform AVBs, leads to a local perturbation in the velocity times square-root-density parameter at the apex of the tube where it will have the largest effect (because the apex is where the largest vibration displacements occur). Detailed local flow field data used in support of the stability ratio evaluations addressed in this report are provided in Section 5.2, below.

Overall Uncertainties Assessment

Based on the above discussions, and the data provided in the following sections, it is concluded that local flow peaking is likely to have contributed significantly to the instability and associated increased vibration amplitude for the failed North Anna tube. Ratios of stresses and stability ratios relative to the North Anna tube, R9C51, are utilized in this report to minimize uncertainties in the evaluations associated with instability constants, local flow field effects and tube damping.

5.2 Tube Damping Data

The damping ratio depends on several aspects of the physical system. Two primary determinants of damping are the support conditions and the flow field. It has been shown that tube support conditions (pinned vs clamped) affect the damping ratio significantly. Further, it is affected by the flow conditions, i.e., single-phase or two-phase flow. These effects are discussed below in more detail.

Reference (5-1) indicates that the damping ratio in two phase flow is a sum of contributions from structural, viscous, flow-dependent, and two-phase damping. The structural damping will be equal to the measured damping in air. However, in two-phase flow, the damping ratio increases significantly and is dependent on the void fraction or quality. It can be shown that the damping contribution from viscous effects are very small.

Damping ratios for tubes in air and in air-water flows have been measured and reported by various authors. However, the results from air-water flow are poor representations of the actual conditions in a steam generator (steam-water flow at high pressure). Therefore, where available, results from prototypic steam-water flow conditions should be used. Fortunately, within the past few years test data on tube vibration under steam-water flow has been developed for both pinned and clamped tube support conditions.

Two sources of data are particularly noteworthy and are used here. The first is a large body of recent, as yet unpublished data from high pressure steam-water tests conducted by Mitsubishi Heavy Industries (MHI). These data were gathered under [ ]^{a,c} tube support conditions. The second is comprised of the results from tests sponsored by the Electric Power Research Institute (EPRI) and reported in References (5-2) and (5-3).

The damping ratio results from the above tests are plotted in Figure 5-4 as a function of void fraction. It is important to note that the void fraction is determined on the basis of [ ]^{a,c}

(Reference (5-4)). The upper curve in the figure is for pinned support conditions. This curve represents a fit to a large number of data points not shown in the figure. The points on the curve are only plotting aids, rather than specific test results.

The lower curve pertains to the clamped support condition, obtained from Reference (5-3). Void fraction has been recalculated on the basis of slip flow. It may be noted that there is a significant difference in the damping ratios under the pinned and the clamped support conditions. Damping is much larger for pinned supports at all void fractions. Denting of the tubes at the top support plate effectively clamps the tubes at that location. Therefore, the clamped tube support curve is used in the current evaluation to include the effect of denting at the top tube support plate.

The Reference 5-3 data as reported show a damping value of .5% at 100% void fraction. The 100% void fraction condition has no two phase damping and is considered to be affected principally by mechanical or structural damping. Westinghouse tests of clamped tube vibration in air has shown that the mechanical damping is only [ ]^{a,c} rather than the .5% reported in Reference (5-3). Therefore the lower curve in Figure 5-4 is the Reference (5-3) data with all damping values reduced by [ ]^{a,c}

5.3 Tube Vibration Amplitudes With [ ]^{a,c} AVB Support

A series of wind tunnel tests were conducted to investigate the effects of tube/AVB eccentricity on the vibration amplitudes caused by fluidelastic vibration.

[

]^{a,c} Prior test results obtained during the past year using this apparatus have demonstrated that the fluidelastic vibration characteristics observed in the tests performed with the cantilever tube apparatus are in good agreement with corresponding characteristics observed in wind tunnel and steam flow tests using U-bend tube arrays. A summary of these prior results is given in Table 5-1.

An overall view of the apparatus is shown in Figure 5-5. Figure 5-6 is a top view of the apparatus. [

]^{a,c}

As shown in Figure 5-7, the tube vibration amplitude below a critical velocity is caused by [

]a,c

Figure 5-7 shows the manner in which the zero-to-peak vibration amplitude, expressed as a ratio normalized to [ ]a,c varies when one gap remains at [ ]a,c For increasing velocities, up to that corresponding to a stability ratio of [

]a,c Figure 5-8 shows typical vibration amplitude and tube/AVB impact force signals corresponding to those obtained from the tests which provided the results shown in Figure 5-7. As expected, impacting is only observed in the [ ]a,c

It is concluded from the above test results that, for a [

]a,c

5.4 Tests to Determine the Effects on Fluidelastic Instability of Columnwise Variations in AVB Insertion Depths

This section summarizes a series of wind tunnel tests that were conducted to investigate the effects of variations in AVB configurations on the initiation of fluidelastic vibration. Each configuration is defined as a specific set of insertion depths for the individual AVBs in the vicinity of an unsupported U-bend tube.

The tests were conducted in the wind tunnel using a modified version of the cantilever tube apparatus described in Section 5.3. Figure 5-9 shows the conceptual design of the apparatus.* The straight cantilever tube, [ ]a,c

[

]a,c

The [
can be individually positioned. The test array has 8 columns and 13 rows with 7 movable AVBs and fixed half width AVBs at the sides of the test section.
]a,c Figure 5-11 shows the AVBs, when the side panel of the test section is removed. Also shown is the top flow screen which is [

]a,c The AVB configurations tested are shown in Figure 5-12. Configuration 1a corresponds to tube R9C51, the failed tube at North Anna. Configuration 2a corresponds to one of the cases in which the AVBs are inserted to a uniform depth and no local velocity peaking effects are expected.

As shown in Figure 5-9, [

]^{a,c}

All the tubes except the instrumented tubed (corresponding to Row 10) are [rigid]^{a,c} As discussed in Section 5.3, prior testing indicates that this situation provides a valid model. The instrumented tube [ ]^{a,c} as shown in Figure 5.10. Its [ ]^{a,c} direction vibrational motion is measured using a non-contacting transducer.

[

]^{a,c} The instrumented tube corresponds to a Row 10 tube as shown in Figure 5-9. However, depending on the particular AVB configuration, it can reasonably represent a tube in Rows 8 through 11. The AVB profile in the straight tube model is the average of Rows 8 and 11. The difference in profile is quite small for these bounding rows.

[ ]^{a,c} using a hot-film anemometer located as shown in Figure 5-9.

Figure 5-13 shows the rms vibration amplitude, as determined from PSD (power spectral density) measurements made using an FFT spectrum analyzer, versus flow velocity for Configuraiton 1b (which corresponds to tube R9C51 in North Anna). Data for three repeat tests are shown and the critical velocity is identified. The typical rapid increase in vibration amplitude when the critical velocity for fluidelastic vibration is exceeded is evident.

The main conclusions from the tests are:

1. Tube vibration below the critical velocity is relatively small, typical of turbulence-induced vibration, and increases rapidly when the critical velocity for the initiation of fluidelastic vibration is exceeded.

2. Configuration 1b (R9C51 in North Anna) has the lowest critical velocity of all the configurations tested.

3. Configuration 1b is repeatable and the configuration was rerun periodically to verify the consistency of the test apparatus.

The initial test results obtained in support of the Beaver Valley Unit 1 evaluation are summarized in Table 5-2. The test data is presented as a velocity peaking ratio; a ratio of critical velocity for North Anna tube R9C51 configuration 1a, to that for each Beaver Valley Unit 1 AVB configuration evaluated.

5.5 References

5-1 [ ]a,c

5-2

5-3

5-4

Table 5-1

Wind Tunnel Tests on Cantilever Tube Model

OBJECTIVE: Investigate the effects of tube/AVB fitup on flow-induced tube vibration.

APPARATUS: Array of cantilevered tubes with end supports [

]a,c

MEASUREMENTS: Tube vibration amplitude and tube/AVB impact forces or preload forces.

RESULTS:

1. [

2.

3.

4.

5.

6.]a,b,c

Table 5-2

Fluidelastic Instability Velocity Peaking Ratios
for Columnwise Variation in AVB Insertion Depths
(Beaver Valley 1)

Type of Insertion Configuration	Peaking Ratio U1a/Un
1a	[ ]a,b,c
1b	
2a	
3	
4a	
4b	
4c	
4d	
4f	
5a	
5b	
5c	
6c	

Note: Un is instability velocity at inlet for type n of AVB insertion configuration.

[ ] a,c

Figure 5-1 Fluidelastic Instability Uncertainty Assessment

U-Bend Test Data

1) MB-3 Tests
   β values of [ ]^{a,b,c}
2) MB-2 Tests
   β of [ ]^{a,b,c}
3) Air Model Tests
   β of [ ]^{a,b,c} without AVBs
   Tendency for β to increase in range of [ ]^{a,b,c} with inactive AVBs (gaps at AVBs)
   Tendency for β to decrease toward a lower bound of [ ]^{a,b,c} with active AVBs

Verification of Instability Conditions

1) Flow conditions at critical velocity from MB-3
2) Measured damping for the specific tube
3) Calculated velocities from ATHOS 3D analysis
4) β determined from calculated critical values
   Good agreement with reported β values
5) ATHOS velocity data with β of [ ]^{a,b,c} and known damping should not significantly underestimate instability for regions of uniform U-bend flow

Figure 5-2 Instability Constant - β

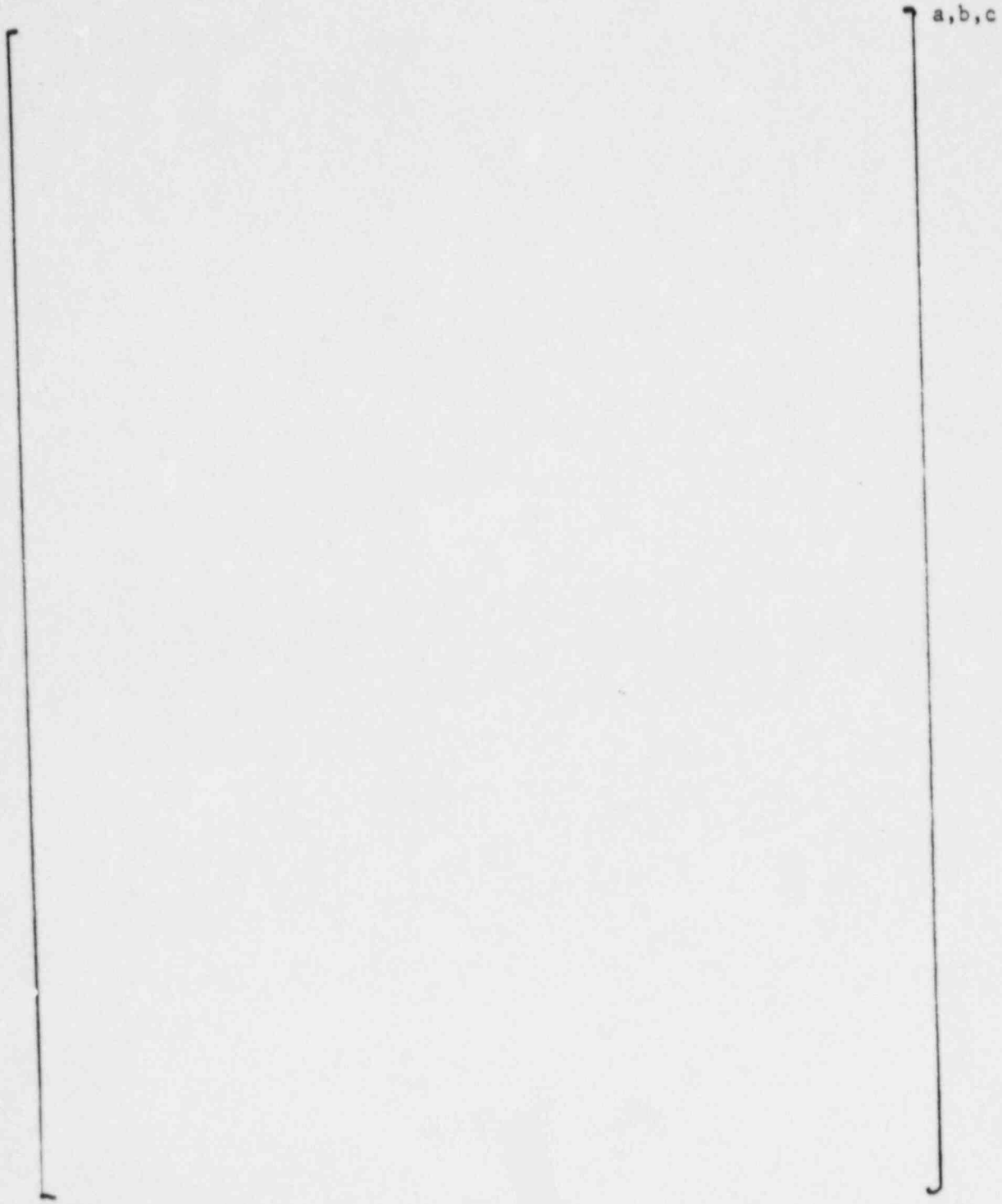

Figure 5-3 Instability Constants, β, Obtained for Curved Tubes from Wind Tunnel Tests on the 0.214 Scale U-Bend Model

[ ]a,b,c

Figure 5-4 Damping vs. Slip Void Fraction

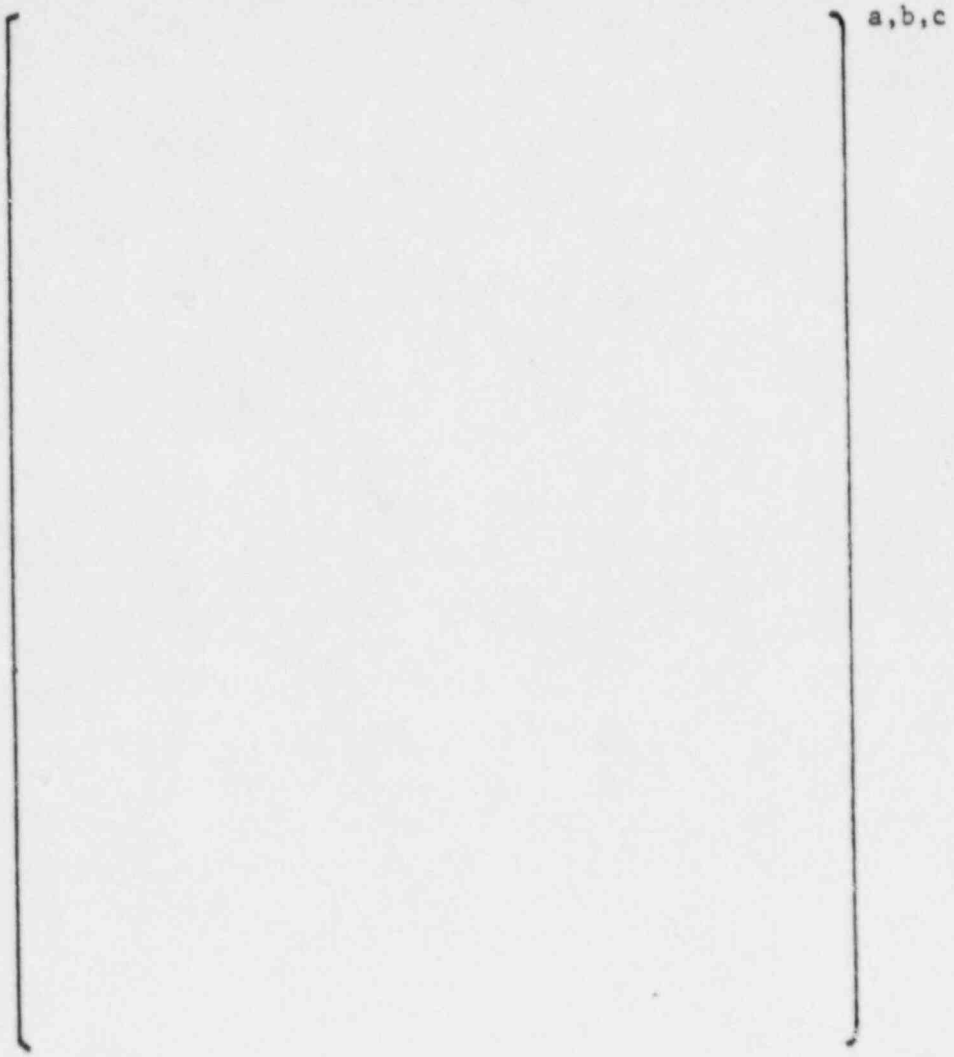

Figure 5-5 Overall View of Cantilever Tube Wind Tunnel Model

Figure 5-6 Top View of the Cantilever Tube Wind Tunnel Model

Figure 5-7 Fluidelastic Vibration Amplitude with Non-Uniform Gaps

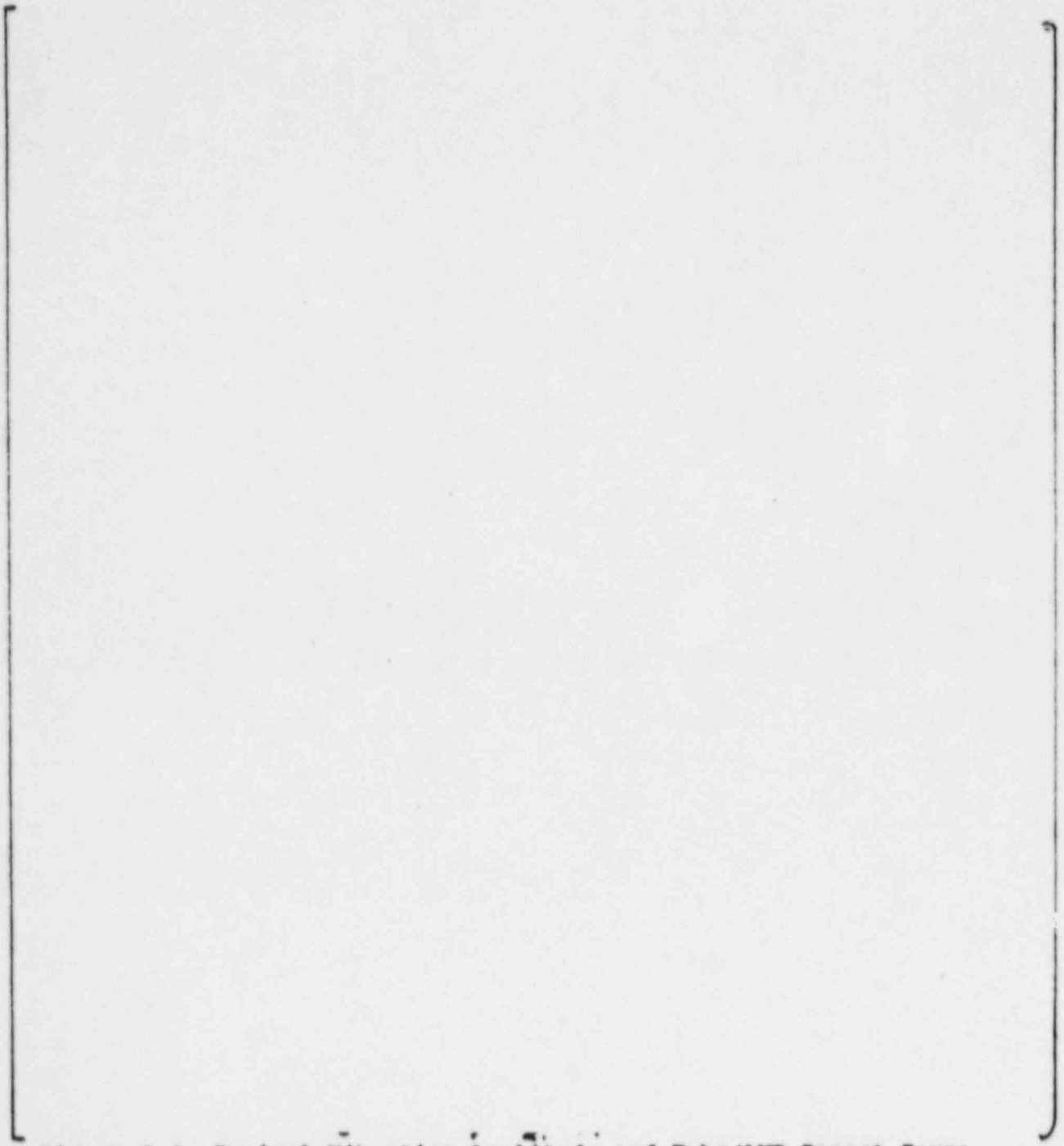

a,b,c

Figure 5-8 Typical Vibration Amplitude and Tube/AVB Impact Force Signals for Fluidelastic Vibration with Unequal Tube/AVB Gaps

[ ] a,b,c

Figure 5-9 Conceptual Design of the Apparatus for Determining the Effects of Fluidelastic Instability of Columnwise Variations in AVB Insertion Depths

[ ]a,b,c

Figure 5-10 Overall View of Wind Tunnel Test Apparatus

[ ]a,b,c

Figure 5-11 Side View of Wind Tunnel Apparatus with Cover Plates Removed to Show Simulated AVBs and Top Flow Screen

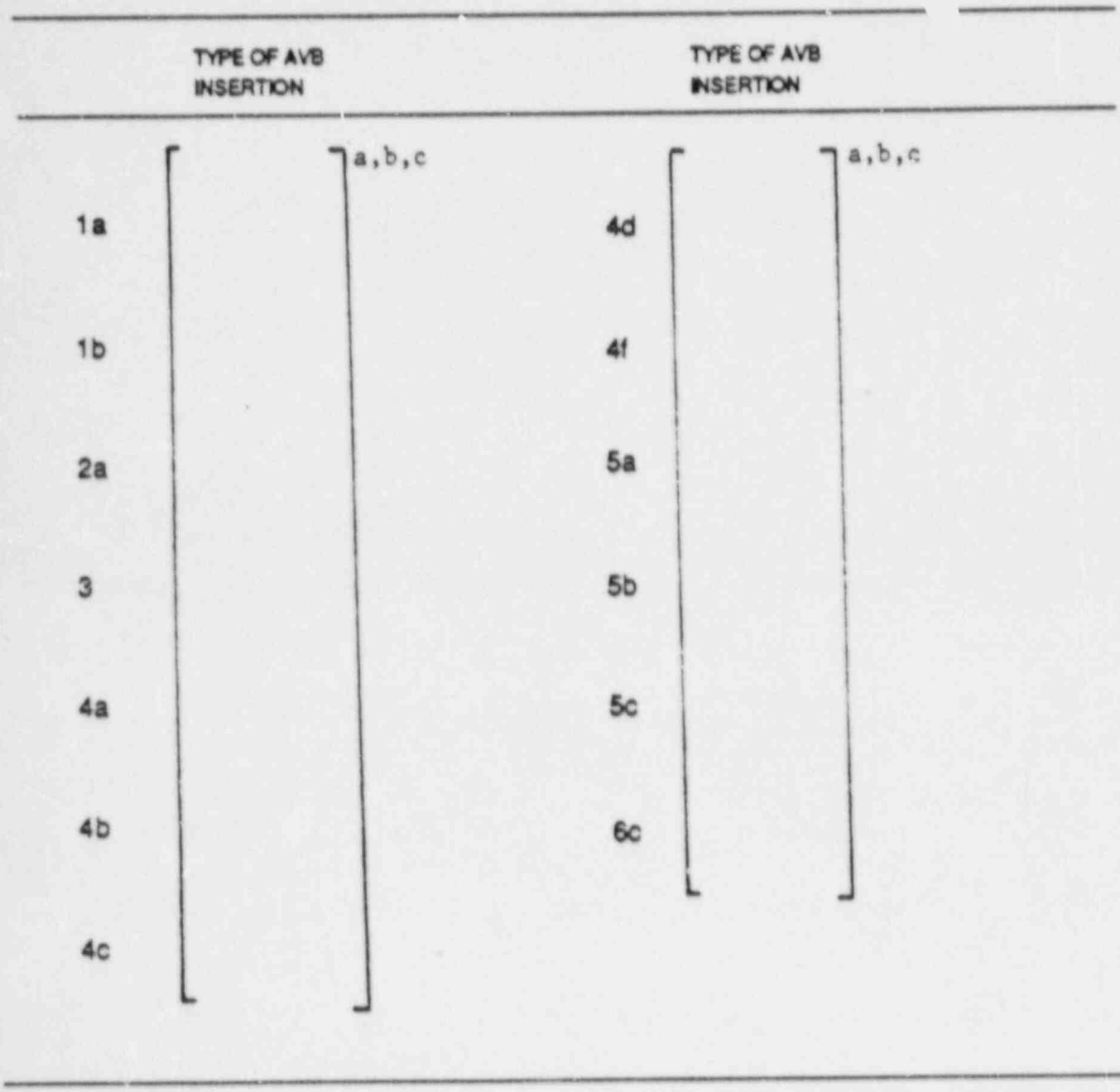

Figure 5-12 AVB CONFIGURATIONS TESTED FOR BEAVER VALLEY 1

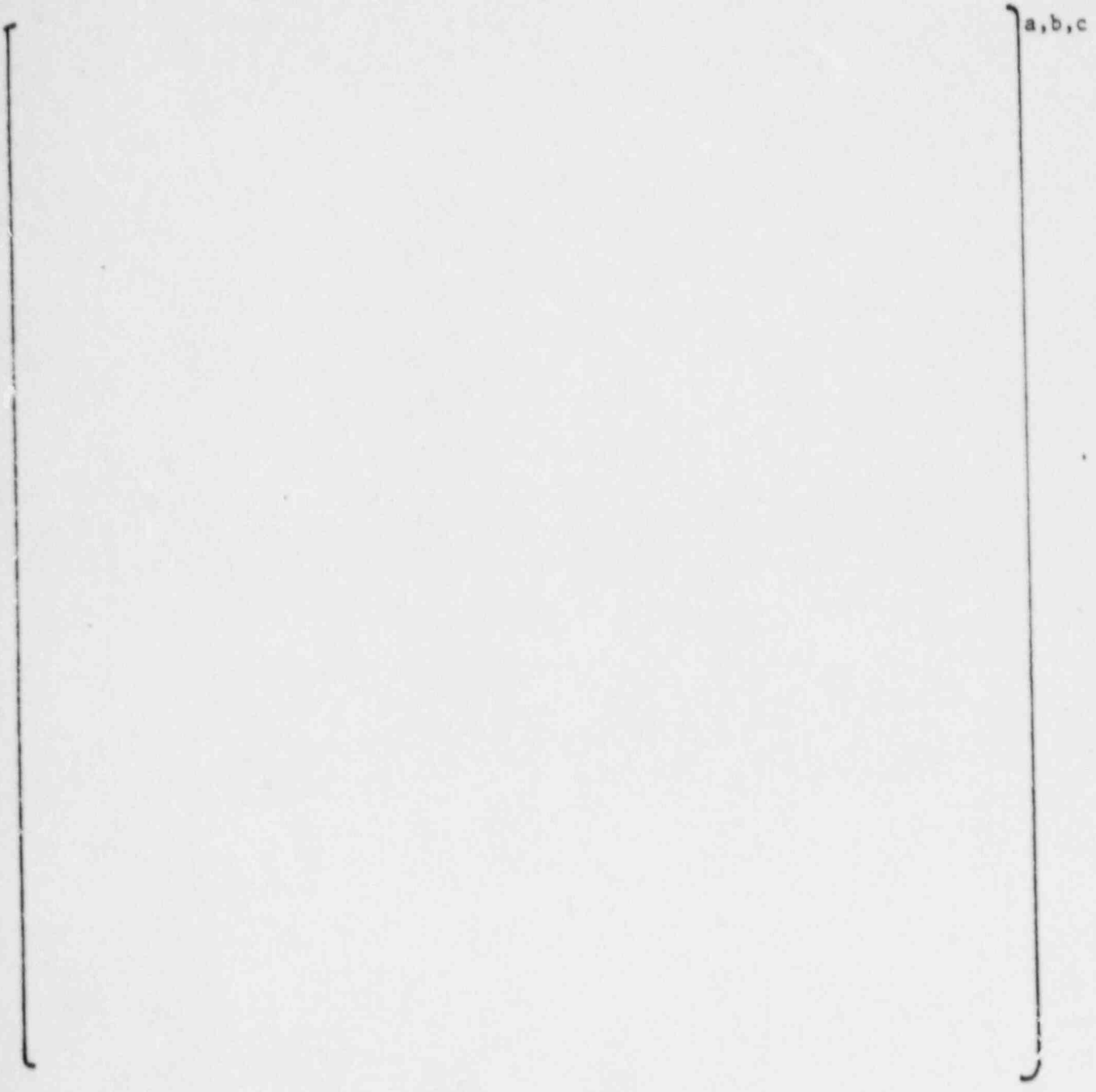

Figure 5-13 Typical Variation of RMS Vibration Amplitude with Flow Velocity for Configuration 1a in Figure 5-12

6.0 EDDY CURRENT DATA AND AVB POSITIONS

6.1 Tube Denting at Top Tube Support Plate

Eddy current data from the 1986 and 1987 outages were examined to evaluate the incidence of corrosion and/or denting at the top tube support plate for the tubes in rows 8 through 12. Because the tube vibration analyses were based on the conservative assumption that all tubes in the area of interest were structurally [ ]^{a,c} in the TSP holes, as if by denting or corrosion, the results of this phase of the examination, which are plotted, are informative, but do not have an impact on the final decision as to whether to plug a tube or not.

6.2 Tube Wall Thinning at the AVB Supports

No tube wall thinning was observed at the tube/AVB intersections in rows 8 through 12 of the bundle.

6.3 Eddy Current Data for AVB Positions

The AVB insertion depths were determined on the basis of interpretation of the eddy current data. To locate the AVBs, the ECT data traces were searched for the characteristic peaks seen in the signals, which indicate the intersection of an AVB (or a true support plate) with the tube (Figure 6.1). The number of these intersection, including zero, were logged for each tube to indicate the presence or absence of AVBs. Where only a single intersection was indicated by the data, the length of this intersection was recorded to provide additional information to assess the adequacy of support for the tube. Figures 6.2, 6.3, and 6.4 show the number of AVB signals found for each tube, as well as the condition of the tube to TSP interface at the locations when it was evaluated.

Since ambiguity can occur in the interpretation of the ECT data, due to inability of ECT to differentiate at which side of a tube a "visible" AVB is located, other information was used to assist in establishing the location of the AVBs. Consistency with the design of the AVB assembly, consistency of data for adjacent columns and verification by [ ]^{a,c} were utilized to determine

the depth of insertion which was plotted. For the cases of [

]a,c

Data from the 1986 outage were the primary data source used to determine the positions of the AVBs. In a few cases, the 'new' tapes from the 1987 outage, which was underway at the time, were reviewed to confirm interpretation of some signals from the '86 tapes. The Eddy Current data analysis was performed principally by the SG Inspection and Analysis group of Westinghouse STD.

6.4 AVB Insertion Depths

AVB position maps for steam generators A through C are given in figures 6.2 through 6.4. The number of visible AVB indications per tube, [ ]a,c of AVB insertion, and the condition of the tube to TSP interface are shown on these figures.

The direct observation data (the number of AVB intersections seen by the eddy current probe) are the principal basis for determining the AVB positions. Where the direct observations were ambiguous or there is a conflict between observations and [ ]a,c the more conservative data are used to determine the AVB positions. Since 'direct observation' gives a 'yes - no' type of answer, the [

]a,c The visual images thus produced being more easily understood when fluid flow peaking situations are evaluated.

Greater conservatism is generally interpreted as the AVB being less inserted although consideration must also be given to the resulting flow peaking factors. No attempt was made to inflate the flow peaking factors through conceptually possible, but unreasonable, interpetation of the data.

6.4.1 AVB Assembly Design

The design of the AVB assembly for the Model 51 Steam Generator includes [

]^{a,c,e} No AVBs are found outside

[ ]^{a,c,e} The [

]^{a,c,e} Review of the eddy current data for Beaver Valley Unit 1 shows that and only in the middle third of the tube bundle, do the lower AVB's not extend as far inward as row 8 or row 9, and typically less than 20 row 10 tubes are not supported.

Eddy current data sometimes indicates the presence of AVBs in column 2 and/or 91. Since [

]^{a,c}

6.4.2 AVB [ ]^{a,c}

The [ ]^{a,c} technique is useful where noisy ECT signals prevent direct observation of the AVBs, where testing is impossible due to plugged tubes, and in some instances to resolve ambiguities in the ECT data. Since [

]^{a,c}

In the case where the AVB characteristic signals can not be confidently determined due to a noisy signal or pre-existing plugged tubes, [

]^{a,c,e}

[

]a,c

6.4.3 [ ]a,c Contact Arc

The adequacy of support provided by [ ]a,c contact indications must be resolved in the cases where a potentially susceptible tube is concerned, since plugging the tube may be required if adequate support cannot be shown. Preliminary analysis indicated that row 10 tubes with peaking factors greater than the failed tube at North Anna, and any tube in rows 11 and 12 were potentially susceptible. Consequently, the primary focus regarding [ ]a,c row contacts was for the tubes in rows 10 through 12.

Arc lengths can be utilized as a basis for determining the support conditions of the tubes when clear [ ]a,c For the tubes in rows 8 through 12, the theoretical contact length of an AVB whose

[ ]a,c inches. In this analysis, a [ ]a,c

[ ]^{a,c} Arc length data was utilized in part to verify the AVB positions in S/G-A at R10C60 and R9C60.

6.4.4 AVB Map Interpretations.

S/G - A

The AVB map for SG-A is given in Figure 6.2. In regions where the potential for high flow peaking factors exists, the tubes in R11C49, 50, and 51, are conservatively assumed to be unsupported based on [ ]^{a,c} to locate the AVB's. The fact that each tube has a [ ]^{a,c} AVB contact signal suggests that they are in fact, most likely supported on one side or the other. AVB's near tube R10C43 are conservatively [ ]^{a,c} contact signals. The resulting flow peaking and tube vibration analyses during the plant outage led to the recommendation that this tube be plugged. Final analysis indicated that plugging of this tube was not necessary. AVB locations around tube R9C60 are based in part on [ ]^{a,c} arc contact readings. (see sec. 6.4.3) The remainder of the AVB plots are based on [ ]^{a,c}

S/G - B

The AVB map for SG-B is given in Figure 6.3. The SG has no unsupported tubes in rows 12 or 11, and one unsupported tube in row 10. The most likely sources of flow peaking factors were the AVB geometries near the tubes in locations R10C47, R9C35, and R9C60. All of these locations were conservatively assumed to be unsupported. None had flow peaking factors high enough to require plugging.

S/G - C

The AVB map for SG-C is given in Figure 6.4. In regions where the potential for high flow peaking factors exists, the tubes in R11C51 and C52; R10C42, 43,

44, 45, 46, 47, 50, 51, 52, and 53; and R9C60 are clearly unsupported. Additionally the tubes in locations R12C51; R11C47; and R10C40, 41, and 60 were conservatively assumed to be unsupported based on [ ]^{a,c} to locate the AVB's. The fact that each of these tubes has a [ ]^{a,c} AVB contact signal suggests that they are in fact, most likely supported on one side of the other. The resulting flow peaking and tube vibration analyses led to the recommendation that the tubes at locations R12C51, R11C47, 51, and 52, and R10C60 be plugged.

6.4.5 Summary of Tube Support Conditions

Resolution of tube support evaluations for single AVB indications are listed in Table 6-1. A summary of unsupported tubes is given in Table 6-2

Table 6.1

Resolution of Tube Support - Tubes With [ ]^{a,c} AVB Indications

A R11C46	[ ]^{a,c}
A R11C49	
A R11C50	
A R11C51	
A R10C41	
A R10C42	
A R10C44	
A R10C45	
A R10C60	
A R9C39	
A R9C40	
A R9C41	
A R9C44	
A R9C60	
B R10C46	
B R10C47	
B R10C46	
B R9C34	
B R9C35	
B R9C40	
B R9C55	
B R9C60	
C R12C51	
C R11C42	
C R11C46	
C R11C47	
C R11C53	
C R10C40	
C R10C41	
C R10C48	
C R10C54	
C R10C60	
C R9C35	
C R9C38	
C R9C39	
C R9C55	
C R9C56	

Tube locations inboard of R9 do not develop sufficiently high flow peaking factors to be of analytical interest.

Table 6.2
Summary Listing of Unsupported Tubes

Steam Generator 'A'

Row 12	No Unsupported Tubes
Row 11	Columns 49, 50, 51
Row 10	Columns 43, 46; and columns 47 through 54,
Row 9	Column 35; and columns 39 through 56
Row 8	Columns 12 through 16; 22 through 27; 29 through 31; 34 through 57; and 60 and 61

Steam Generator 'B'

Row 12	No Unsupported Tubes
Row 11	No Unsupported Tubes
Row 10	No Unsupported Tubes
Row 9	Column 35; columns 42 through 55; and 60
Row 8	Columns 10, 11, 12, 34, 35, 38 through 57; 60, 61 79, 82, 83, 92, and 93

Steam Generator 'C'

Row 12	Column **51**
Row 11	Columns **47**, **51**, **52**
Row 10	Columns 40 through 47; 50 through 54; and **60**
Row 9	Columns 39 through 54; and **60**
Row 8	Columns 35; columns 38 through 56; 60 and 61

Analysis indicates that tubes shown in **boldface type** require plugging for susceptibility to North Anna rupture event.

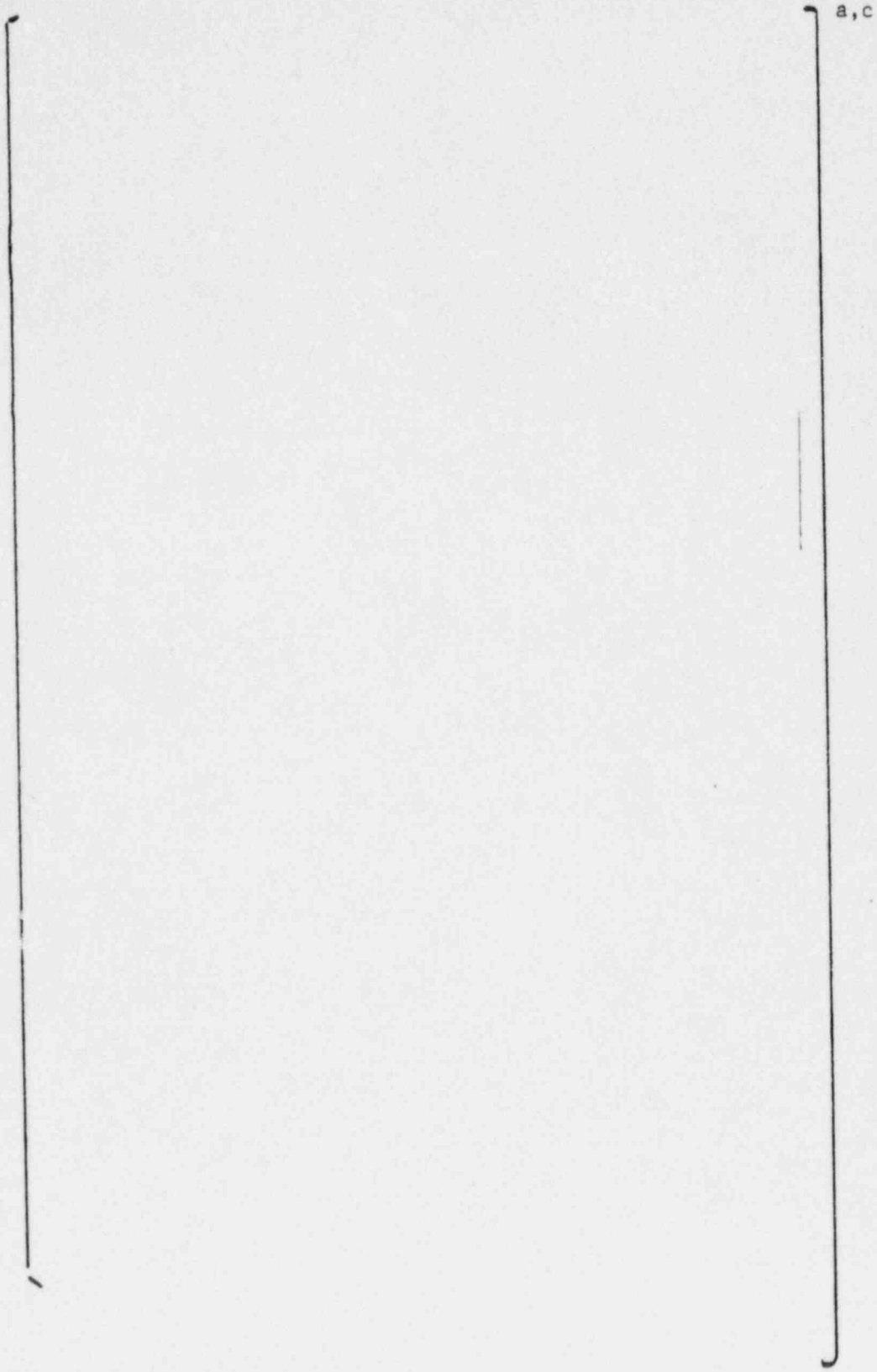

Figure 6-1 AVB Insertion Depth Confirmation

51 Series Steam Generator
Beaver Valley # 1
SG - A

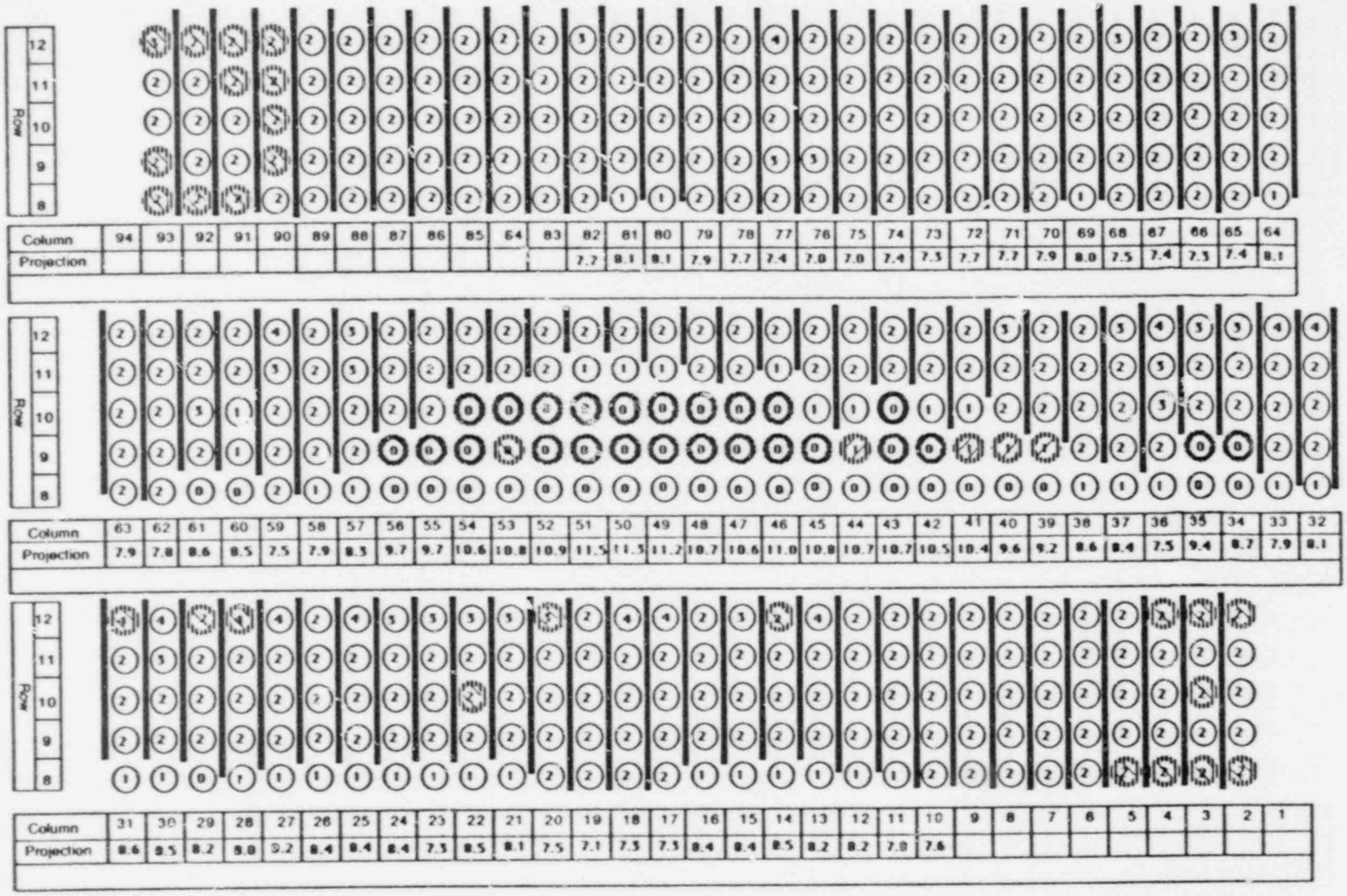

Figure 6-2: Beaver Valley Unit 1 Steam Generator A - AVB Positions

51 Series Steam Generator
Beaver Valley # 1
SG - B

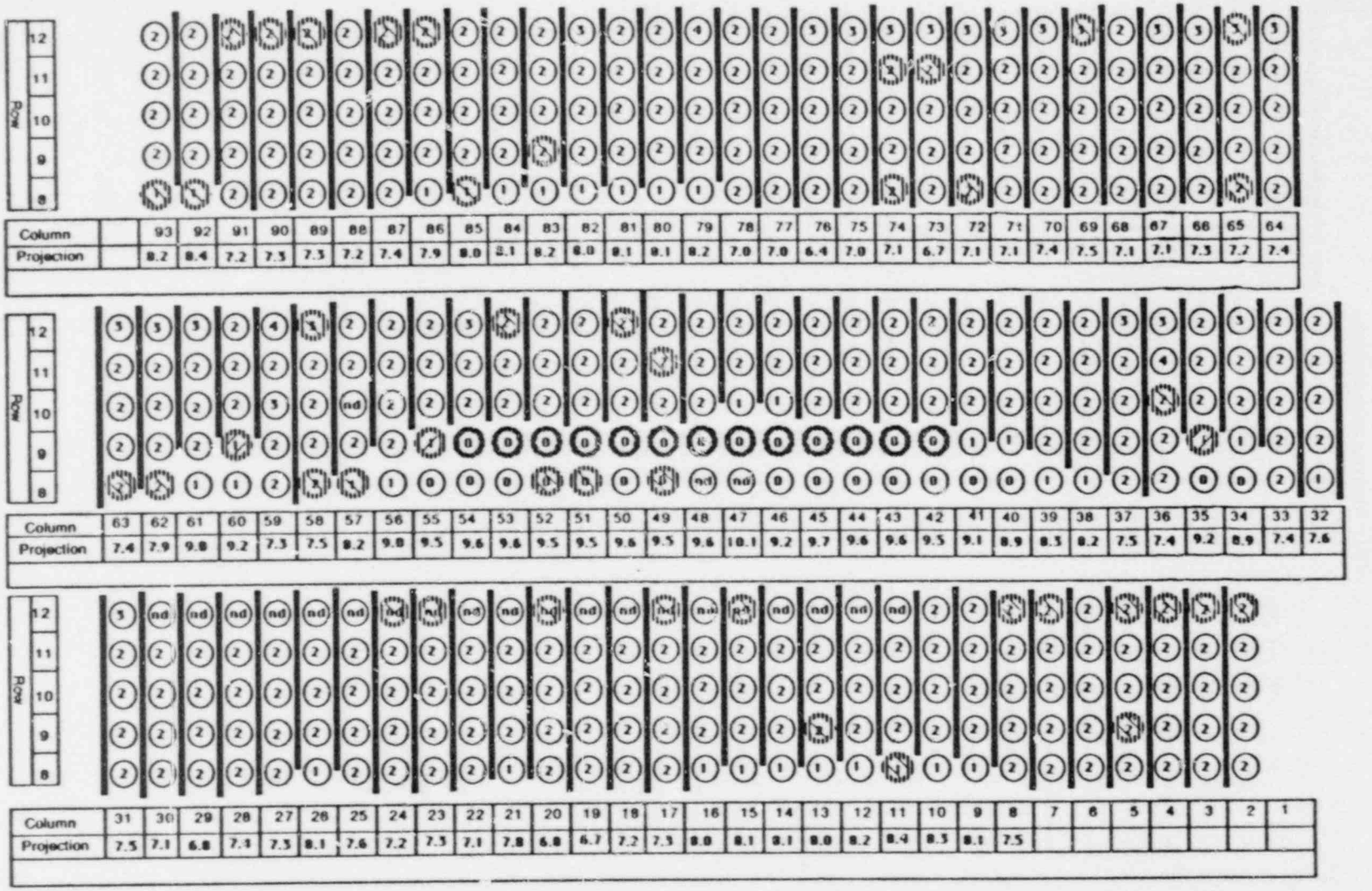

NOTES:

Numbers indicate 'visible' AVB's

If no number is given, no data exists

[ ]a,c

Tube inspected and found dented with deformation at upper TSP

Tube inspected and found corroded with magnetite at upper TSP

Recommend tube be plugged for susceptibility to 'North Anna' type tube rupture

Tube inspected and found to have no detectable degradation at TSP # 7

(nd) Noisy data; inconclusive data

03/23/88
BWY

Figure 6 - 3: Beaver Valley Unit 1 Steam Generator B - AVB Positions

51 Series Steam Generator
Beaver Valley # 1
SG - C

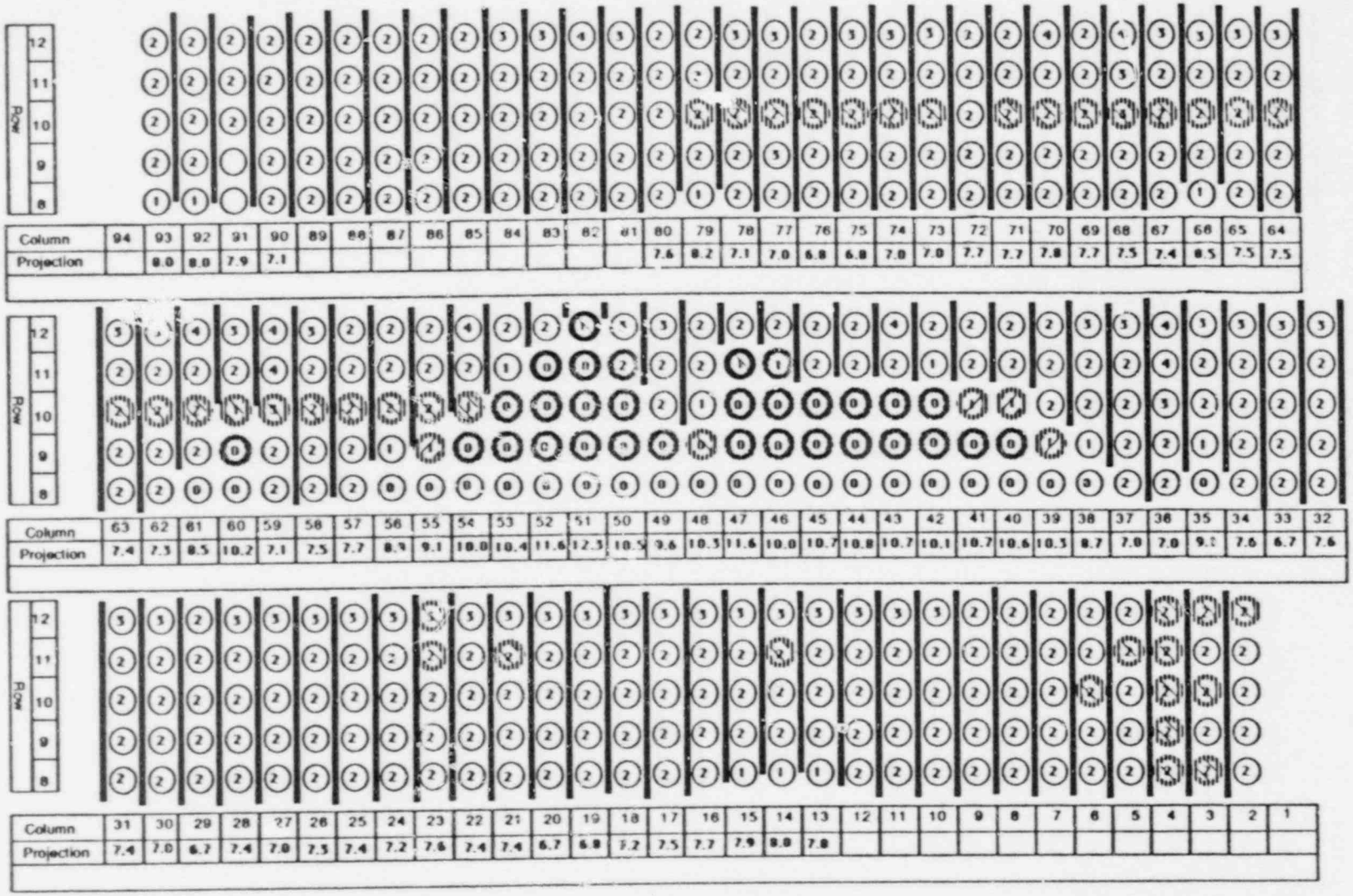

Figure 6 - 4: Beaver Valley Unit 1 Steam Generator C - AVB Positions

7.0 THERMAL AND HYDRAULIC ANALYSIS

This section presents the results of a thermal and hydraulic analysis of the flow field on the secondary side of the steam generator using the 3-D ATHOS computer code, Reference (7-1). The major results of the analysis are the water/steam velocity components, density, void fraction, and the primary and secondary fluid and tube wall temperatures. The distributions of the tube gap velocity and density along a given tube were obtained by reducing the ATHOS results. In the following subsections, the ATHOS model and some sample results of the analysis are described.

Because of the staggered anti-vibration bar insertion configurations, local flow peaking occurs at certain tubes in the U-bend. Its effect on tube gap velocity perturbation was obtained using test data and applied to the Beaver Valley Unit 1 steam generators. Normalized stability ratios over the operating history of the plant were determined based on the reported plant operating history. The results of these investigations are also presented in this section.

7.1 Beaver Valley Unit 1 Steam Generator Operating Conditions

Recent steam generator operating condition data for Beaver Valley Unit 1 was provided by Duquesne Light. The data covered the period from October 8, 1986 to July 22, 1987 within fuel cycle 6. A review of the data was completed to select a set of representative operating conditions on which to base the ATHOS flow field evaluation. The selected conditions are for data for generators B/C, which operated with slightly higher power than generator A. An average core power level of 99.6% of full power was selected, generators B or C were producing approximately 887 MWt each which is equal to the nominal power rating. Table 7-1 summarizes these data along with other thermal/hydraulic parameters which are germane to the ATHOS evaluation.

With these data calculations were completed using the Westinghouse GENF computer code to verify the plant data and to establish a complete list of operating conditions required for the ATHOS analysis. The GENF code determines the primary side temperatures and feedwater flow rate required to obtain the specified steam pressure at the given power rating. Besides confirming these parameters, the code calculates the circulation ratio which is of primary importance since it establishes the total bundle flow rate and average loading on the tubes. The operating conditions utilized in the ATHOS 3-D analysis are shown in Table 7-2.

7.2 ATHOS Analysis Model

The calculation of relative stability ratios involves comparing the stability ratio calculated for one or more tubes in a given plant to the ratio calculated for the ruptured Row 9/Column 51 tube in the North Anna Series 51 steam generator. It makes use of ATHOS computed flow profiles for both tube bundles. Since the presence of AVBs in the U-bend region of a tube bundle could influence the overall flow field and/or the local flow parameters for a particular tube of interest, some discussion of the treatment of AVB's is necessary before presenting a description of the ATHOS model.

The ATHOS code does not include the capability to model the presence of the AVBs in the U-bend region. However, Westinghouse has modified the code to include the capability to model the AVBs at a uniform depth of insertion via

[

]a,c

[

]a,c

This methodology has been utilized in the Beaver Valley Unit 1 analysis.

The ATHOS analysis model for the Beaver Valley 1 steam generator consists of

[

]a,c Figures 7-1 and 7-2 show the plan and the elevation views of the model, respectively. These two figures show the layout of the flow cells and identify locations for some of the geometric features.

Figure 7-3 reproduces the plan view of the model but with the tube layout arrangement superimposed. This figure illustrates the locations of the tubes in the various flow cells. [

]a,c

7.3 ATHOS Results

The results from the ATHOS analysis consist of the thermal-hydraulic flow parameters necessary to describe the 3-D flow field on the secondary side of the steam generator plus the distributions of the primary fluid and mean tube wall temperatures. Since the velocity components computed by ATHOS are defined on the surfaces of a flow cell, the tube gap velocity and density distributions along a particular tube required for tube vibration evaluation are determined by a post-processor from the ATHOS output. The post-processor generates a data file which contains this information for all the tubes in the model and the file serves as part of the input data required for tube vibration analyses. Because the majority of the flow cells contain more than one tube inside a cell, the tube gap velocity and density surrounding a tube are obtained by interpolation of the ATHOS calculated velocities (defined on the cell surfaces) and density (defined at the center of the cell). The post-processor performs the necessary interpolations to determine in-plane and out-of-plane velocities at specific intervals along the length of the tubes.

Figure 7-4 shows a vector plot of the flow pattern on the vertical plane of symmetry of the steam generator (the vectors are located at the center of the flow cells shown in Figure 7-2). It is seen that in the U-bend region the mixture turns radially outward, normal to the curvature of the bends toward the region of least flow resistance (i.e., outside the dome formed by the U-bends). Figure 7-5 shows the resultant vectors of the radial and circumferential velocity components on the horizontal plane at Z = 21, the sixth plane above the top tube support plate (see Figure 7-2). The radial outward flow is more evident from this figure since it ignores the axial component. It may be noted that the radial velocity at this axial location is low at the center of the bundle and increases with radius. Figure 7-4 shows that the axial component is about four times greater than the radial component. Figure 7-6 shows the flow pattern (resultant of the radial and circumferential components) on top of the tubesheet. Because of the thermal syphon action (resulting from the higher heat flux and vapor generator in the hot leg), a portion of the cold leg side fluid flows to the hot leg side before turning upward. The relatively high in-flow velocity along the tubelane from the wrapper opening is also evident.

Figures 7-7, 7-8 and 7-9 show a sample of the individual tube gap velocity and density distributions along three tubes at Row 10. In each figure the gap velocity and density along the length of the tube are plotted from the hot leg tubesheet end on the left of the figure to the cold leg end on the right. Figure 7-10 shows the plot of the average in-plane gap velocity normal to the tube and density profiles as a function of the column number along Row 10. The average values were taken as the numerical average of the parameter over the entire 180° span of a U-bend at a given column location. The average velocity is seen to be relatively [

]^{a,b,c}

7.4 Relat[illegible] Stability Ratio Over Operating History

One aspect of the evaluation of the Beaver Valley 1 steam generators is to examine the operating history data and use it to determine the susceptibility to fatigue from fluidelastic vibration resulting from the 11+ years of operation. This assessment has been completed through the use of a parameter termed the normalized stability ratio. The normalized stability ratio compares the fluidelastic stability ratio for each period of a plant's operation (fuel cycle) to a reference stability ratio based on a recent operating condition. A plot of this ratio against operating time, therefore, provides a relative indication of the effect of past operation on the plant's fluidelastic stability ratio. This normalized time-dependent ratio is subsequently combined with an absolute stability ratio for the reference operating point derived from detailed three-dimensional thermal/hydraulic and tube vibration calculations. High values for the net stability ratio, in particular, over a significant period of operation, coupled with other prerequisite conditions (e.g., absence of AVB support and denting at the top tube support plate), could indicate an increased susceptibility to fluidelastic vibration instability and fatigue.

The fluidelastic stability ratio is defined as the ratio of the effective fluid velocity acting on a given tube to the critical velocity at which large amplitude fluidelastic vibration initiates:

$$\text{Fluidelastic Stability Ratio, SR} = \frac{U_{effective}}{U_{critical\ at\ onset\ of\ instability}}$$

In this ratio, the effective velocity depends on the distribution of flow velocity and fluid density, and on the mode shape of vibration. The critical velocity is based on experimental data and has been shown to be dependent upon the tube natural frequency, damping, the geometry of the tube, the tube pattern, and the fluid density, along with the appropriate correlation coefficients.

The detailed calculation of this ratio using velocity and density distributions, etc., requires three-dimensional thermal hydraulic and tube vibration calculations which are very time consuming. Alternately, a simplified, one-dimensional version of this ratio has been used to provide a more rapid, relative assessment technique for determining the effect of past operation on the stability ratio. The normalized stability ratio is defined by the following equation:

[ ]a,c

In this equation "cyc x" refers to each fuel cycle and "ROP" to the recent operating condition. While this simplified approach cannot account for three-dimensional tube bundle effects, it does consider the major operational parameters affecting the stability ratio. Four components make up this ratio: a loading term based on the dynamic pressure (ρV^2), a tube incremental mass(m) term, the natural frequency of the tube (f_n), and a damping ratio (δ) term. It should be noted that the ratio is relative, in that each

component is expressed as a ratio of the value for a given fuel cycle to that of the recent operating point.

[

]^{a,c} The particular damping correlation which is used for all normalized stability ratio calculations is based on a dented condition at the top tube support plate (a [ ]^{a,c} condition, as discussed in Section 5.2). The [ ]^{a,c} condition is also assumed in calculating the tube natural frequency.

As discussed previously in Section 7.1, the reference stability ratio calculation for the Beaver Valley 1 generators was based on the following operating parameters which are for a recent operating point in cycle 6 as supplied by Duquesne Light:

Steam Flow	3.90×10^6 lbm/hr
Steam Pressure	837 psia
Circulation Ratio	[ ]^{a,c} (Westinghouse calculation)

A series of calculations were completed to generate a normalized stability ratio for each of the six fuel cycles since the plant became operational in June 1976. Data for this evaluation is summarized in Table 7-3. Included are cycle average values for full load steam pressure and primary fluid average temperature. The number of days that the plant has operated above 85% of full power are also listed. Since tube vibration and possible fatigue are associated with operation at close to 100% power, only these higher power operating periods are considered important to the evaluation. The operating parameters listed in Table 7-3 were then input to the Westinghouse "GENF"

computer code to determine the overall performance of the steam generator, in particular, the circulation ratio for each fuel cycle. These calculated values are also listed in the table.

The resulting normalized stability ratios are shown in Figure 7-11. In this figure, the normalized stability ratio for each fuel cycle is plotted against cumulative operating time above 85% power. Note that the ratio assigned to each of the high power intervals listed in Table 7-3 (85-90%, 90-95%, and 95-100%) and plotted in Figure 7-11 has been conservatively based on the highest power level in each interval. Figure 7-11 indicates that the full power normalized ratio has been a nearly constant throughout operation. However, small cycle-to-cycle variation which is predicted is related to changes in steam pressure; higher pressures yield lower stability ratios and vice versa. Higher steam pressures result in higher U-bend density, lower U-bend velocity, and increased damping as a result of lower voids in the U-bend. The higher damping, together with decreased loading on the tubes, result in the lower normalized stability ratio which is indicated, for example, in cycle 6. Figure 7-11 also shows that the stability ratios and operating periods at the lower power intervals are negligible compared to the full power results and could have been disregarded in the analysis.

References

7-1 [ ] a,c

Table 7-1

Beaver Valley 1 Steam Generator Operating Conditions

Power	887 of 825 MWT
Steam Pressure	837 psia
Feedwater Flow Rate	3.90×10^6 lbm/hr
Feedwater Inlet Temperature	435.5°F
Water Level	44% of Narrow Range Span (Assumed)
Primary Inlet Temperature	604.5°F
Primary Outlet Temperature	546°F

Table 7-2
Steam Generator Operating Conditions Used for
ATHOS Analysis

Power	887 MWT
Primary Flow Rate	3.60×10^7 lb/hr
Primary Inlet Temperature	604.5°F
Primary Outlet Temperature	546 °F
Feedwater Flow Rate	3.90×10^6 lb/hr
Feedwater Inlet Temperature	435.5°F
Water Level from Tubesheet	505.9 inches
Steam Pressure	837 psia
Circulation Ratio	4.99

Table 7-3
Beaver Valley Unit 1 Operating History Data

Cycle	Beginning	End	Days at Each Power Level 80-90%	90-95%	90-100%	Full Load* Steam* Pressure (psia)	TAVG* (Deg F)	Calculated Circ. Ratio
1	14-JUN-76	30-NOV-79	29	39	223	829	573	[a,c]
2	20-NOV-86	25-DEC-8	24	37	159	835	573	
3	09-JUL-82	10-JUN-83	8	22	241	834	573	
4	24-SEP-83	11-OCT-84	8	8	297	824	574	
5	04-JAN-85	17-MAY-86	13	20	331	822	574	
6	25-AUG-86	11-DEC-87	16	7	364	837	576	
			98	133	1615			

* For SG B

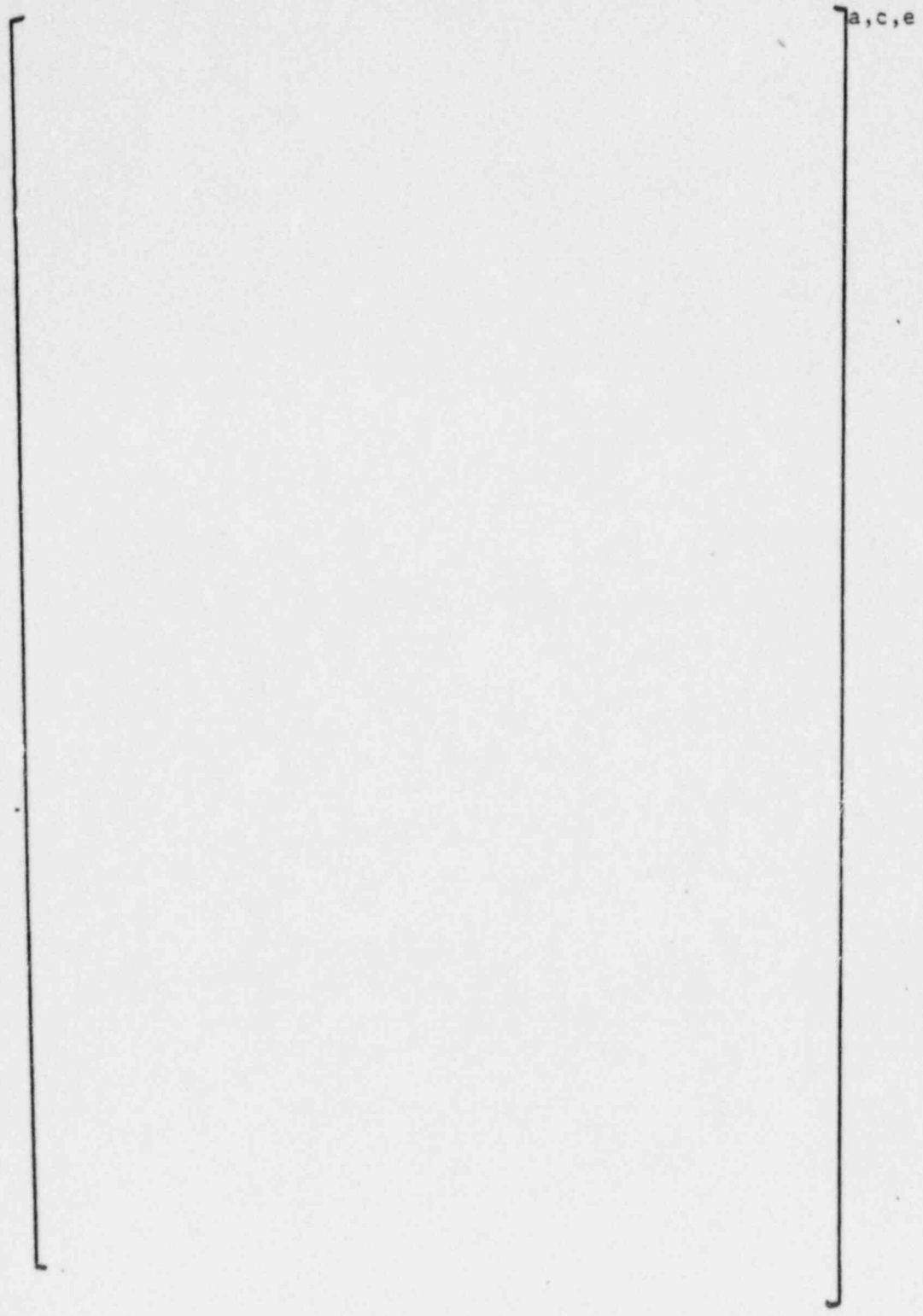

Figure 7-1 Plan View of ATHOS Cartesian Model for Beaver Valley 1

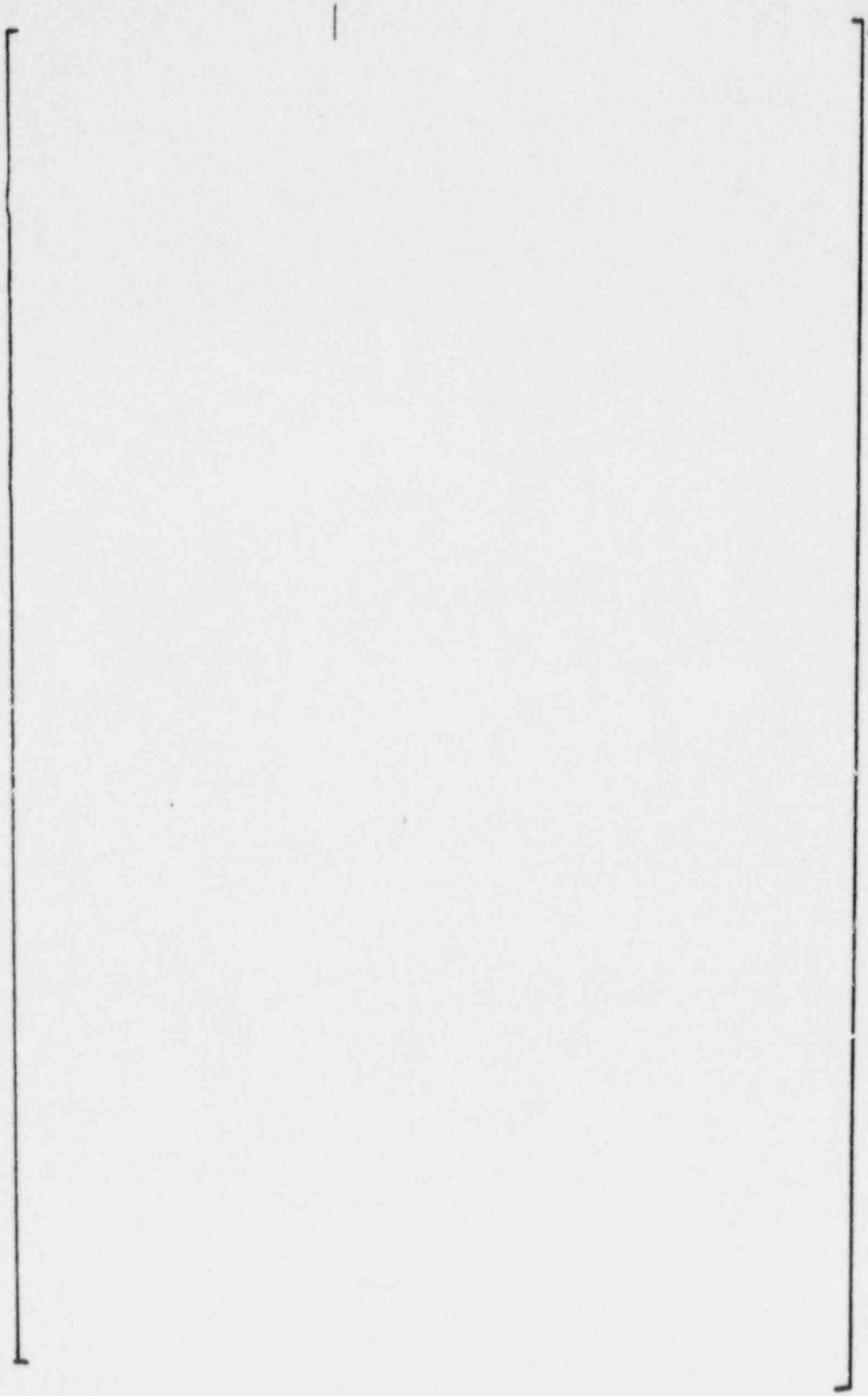

Figure 7-2 Elevation View of ATHOS Cartesian Model for Beaver Valley 1

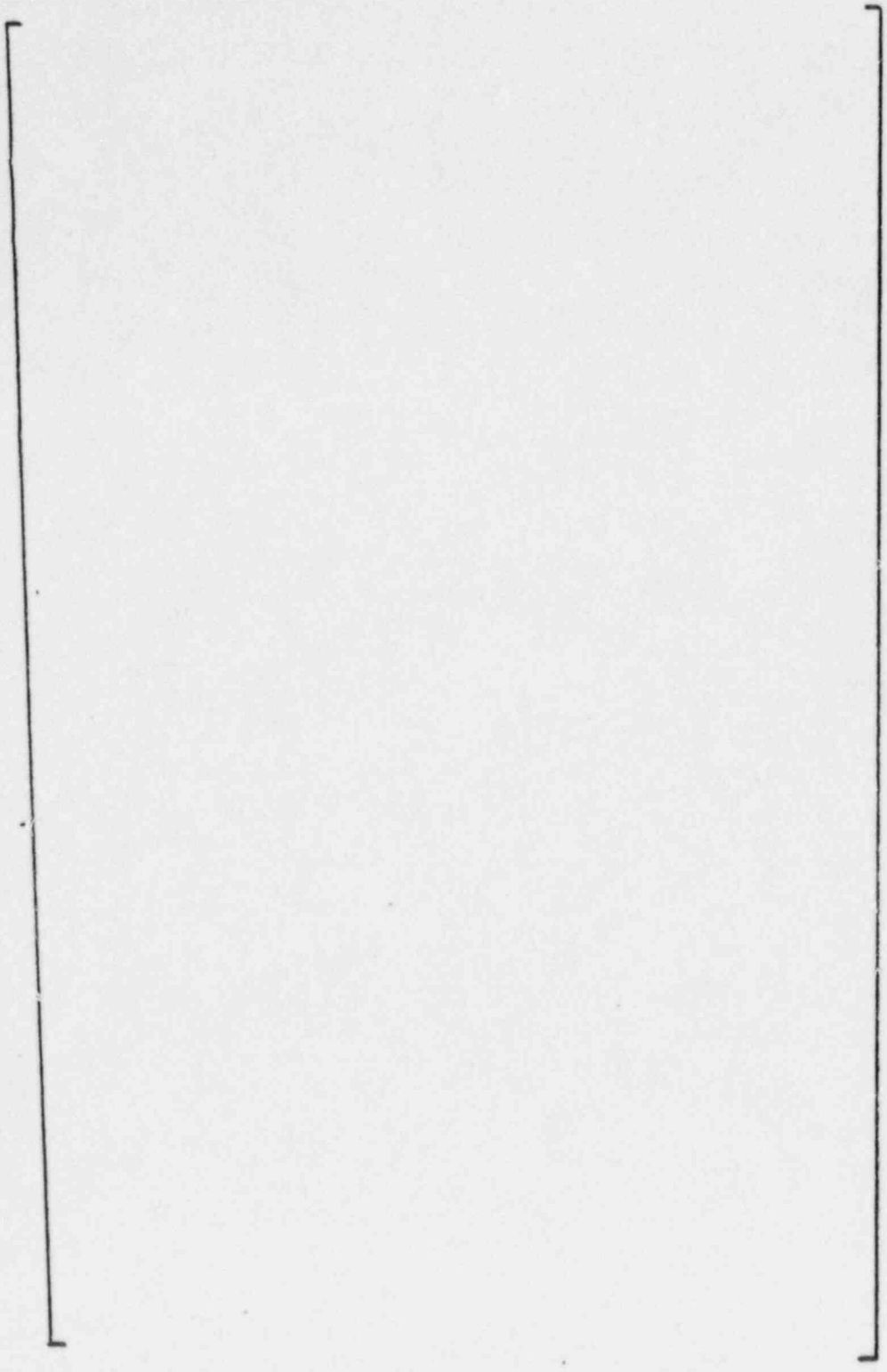

Figure 7-3 Plan View of ATHOS Cartesian Model for Beaver Valley 1 Indicating Tube Layout

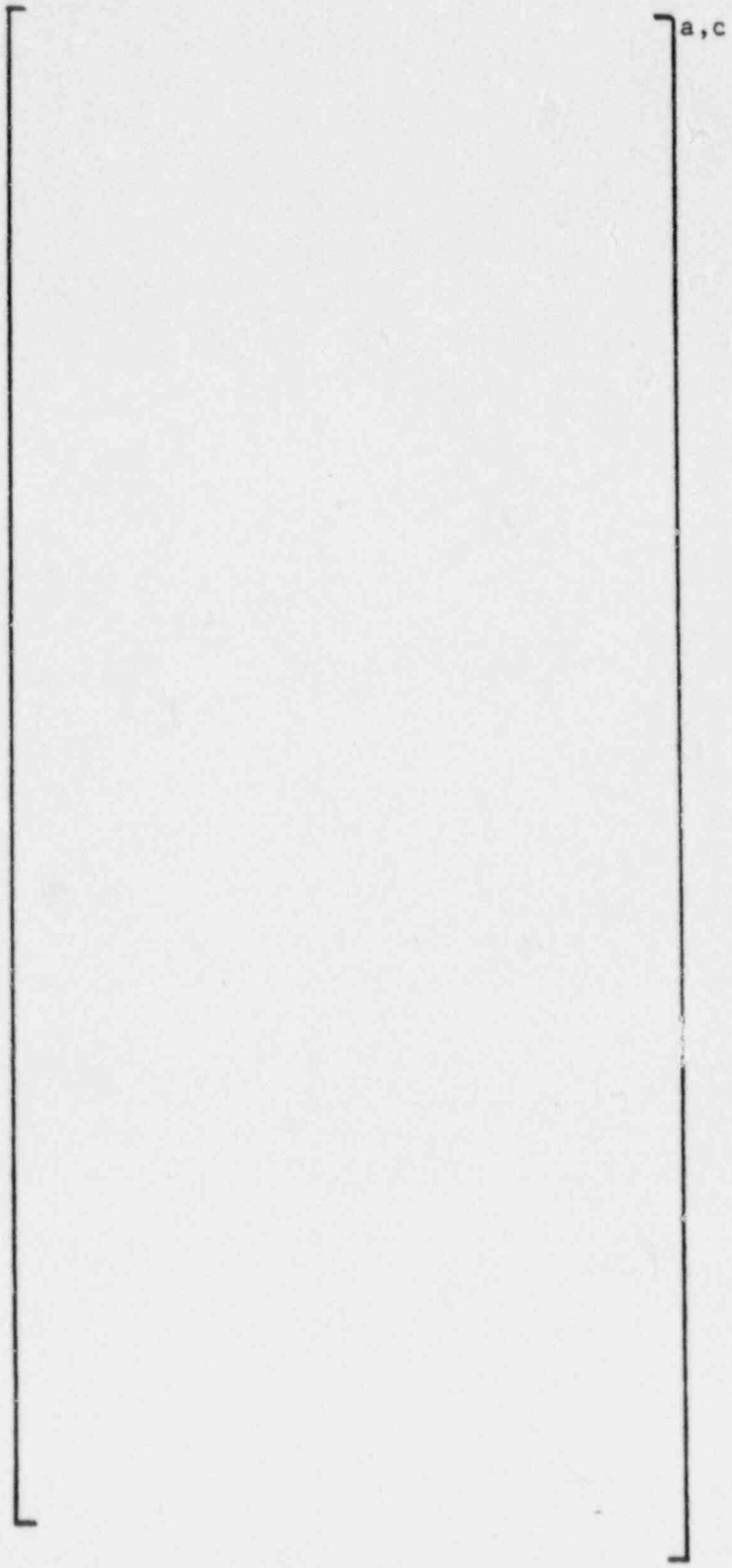

Figure 7-4 Flow Pattern on Vertical Plane of Symmetry

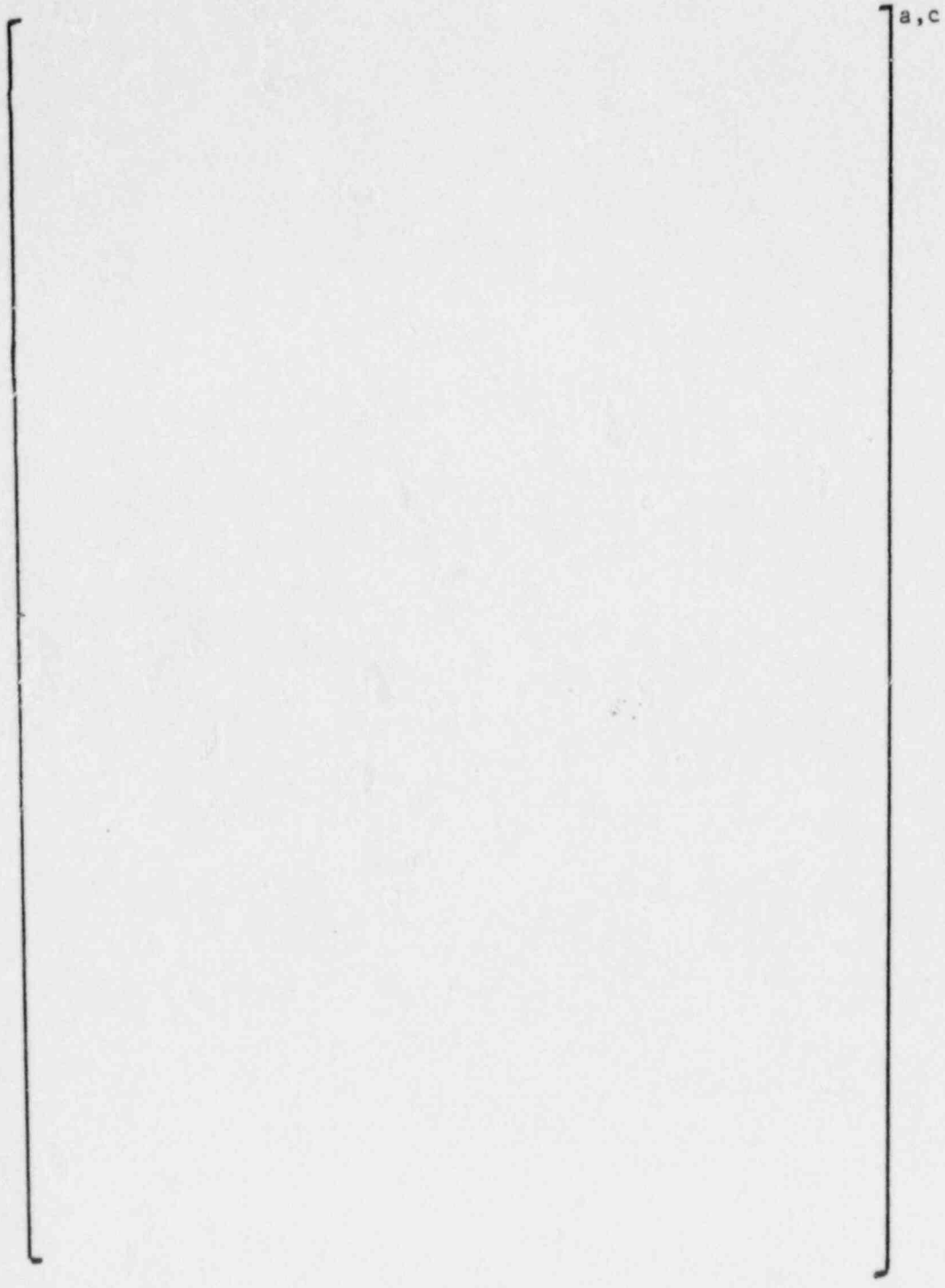

Figure 7-5 Lateral Flow Pattern on a Horizontal Plane in the U-Bend Region

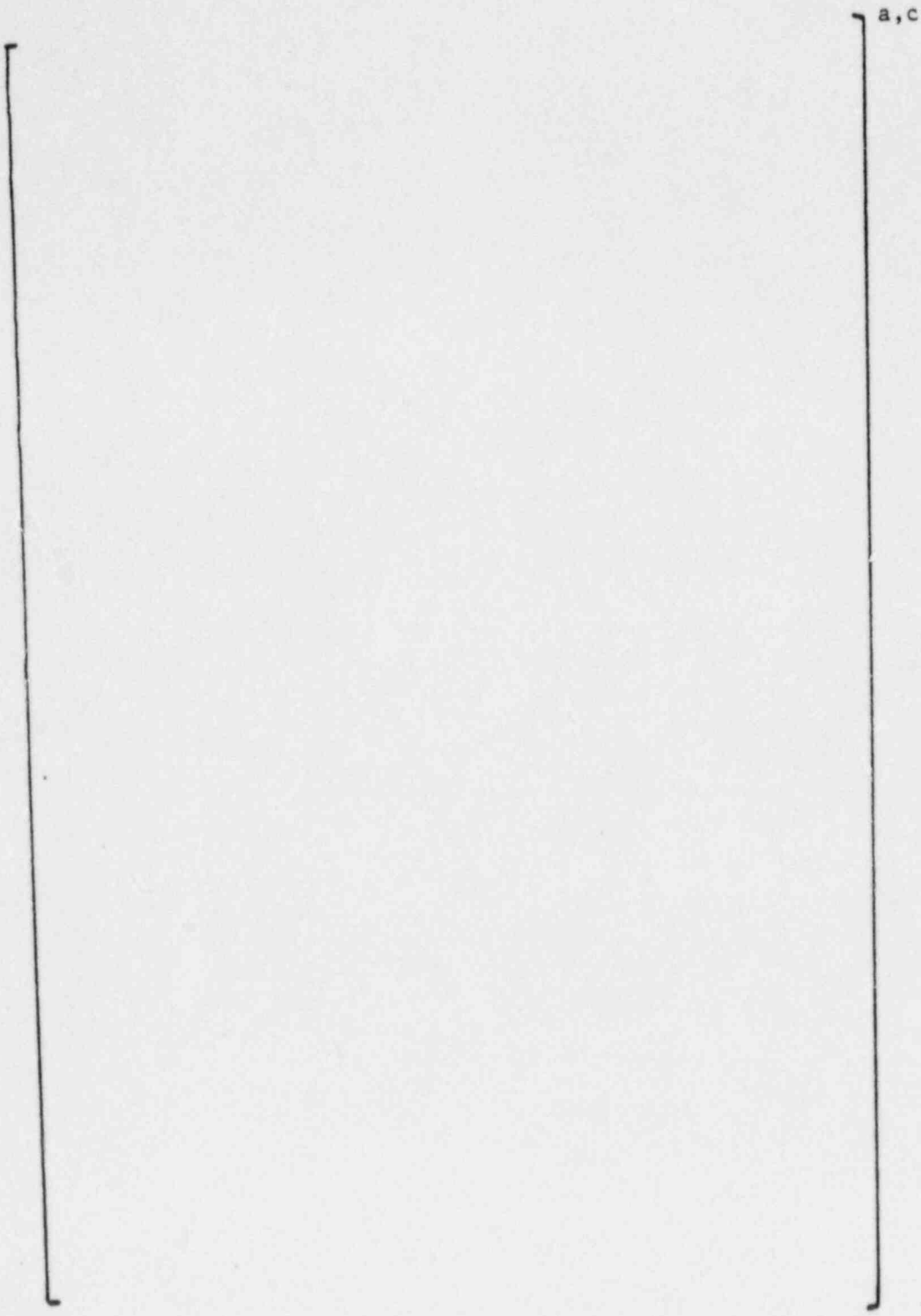

Figure 7-6 Lateral Flow Pattern on Top of Tubesheet

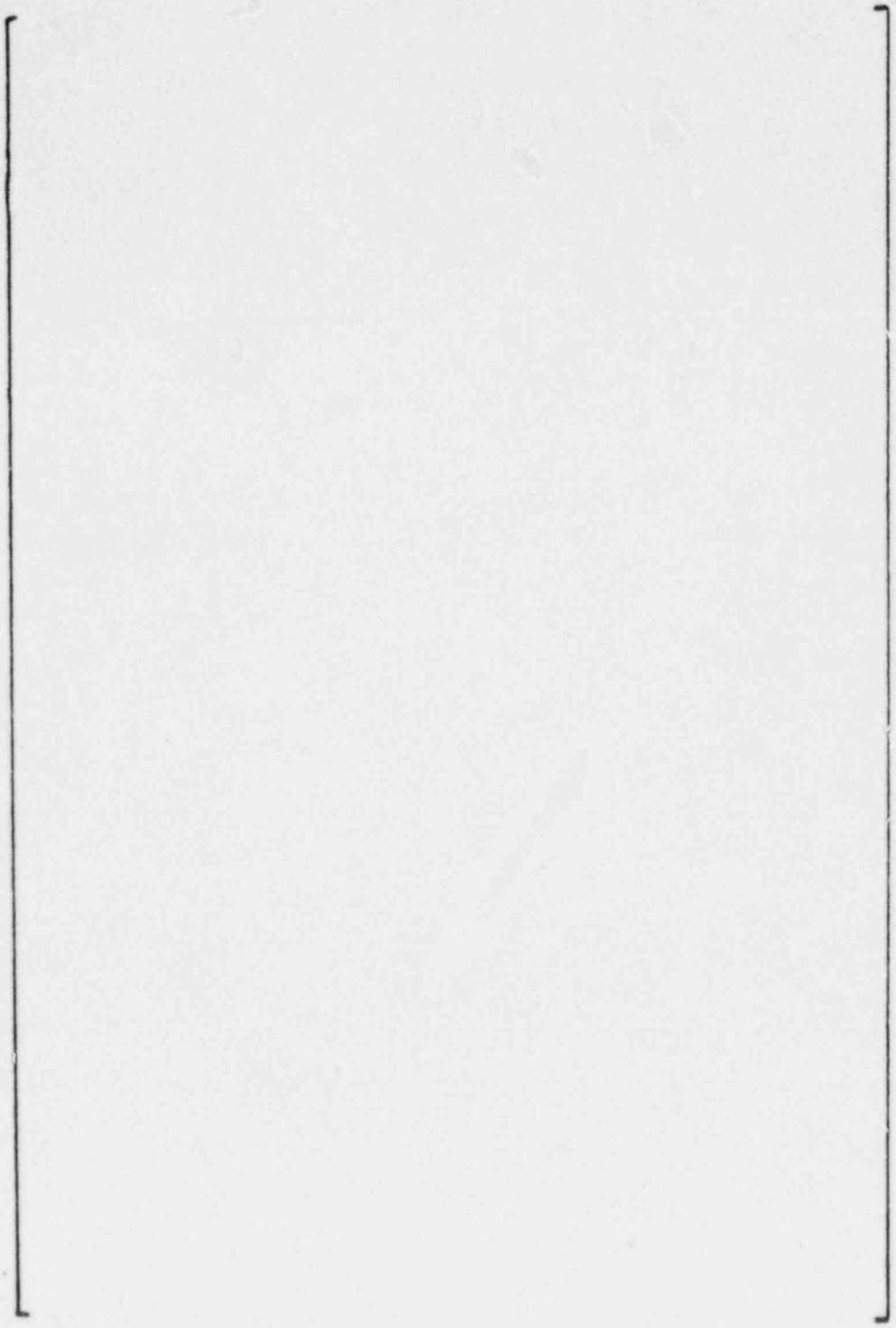

Figure 7-7 Tube Gap Velocity and Density Distributions for Tube Row 10/Column 3

[ ]a,c

Figure 7-8 Tube Gap Velocity and Density Distributions for Tube Row 10/Column 20

[ ] a,c

Figure 7-9 Tube Gap Velocity and Density Distributions for Tube Row 10/Column 40

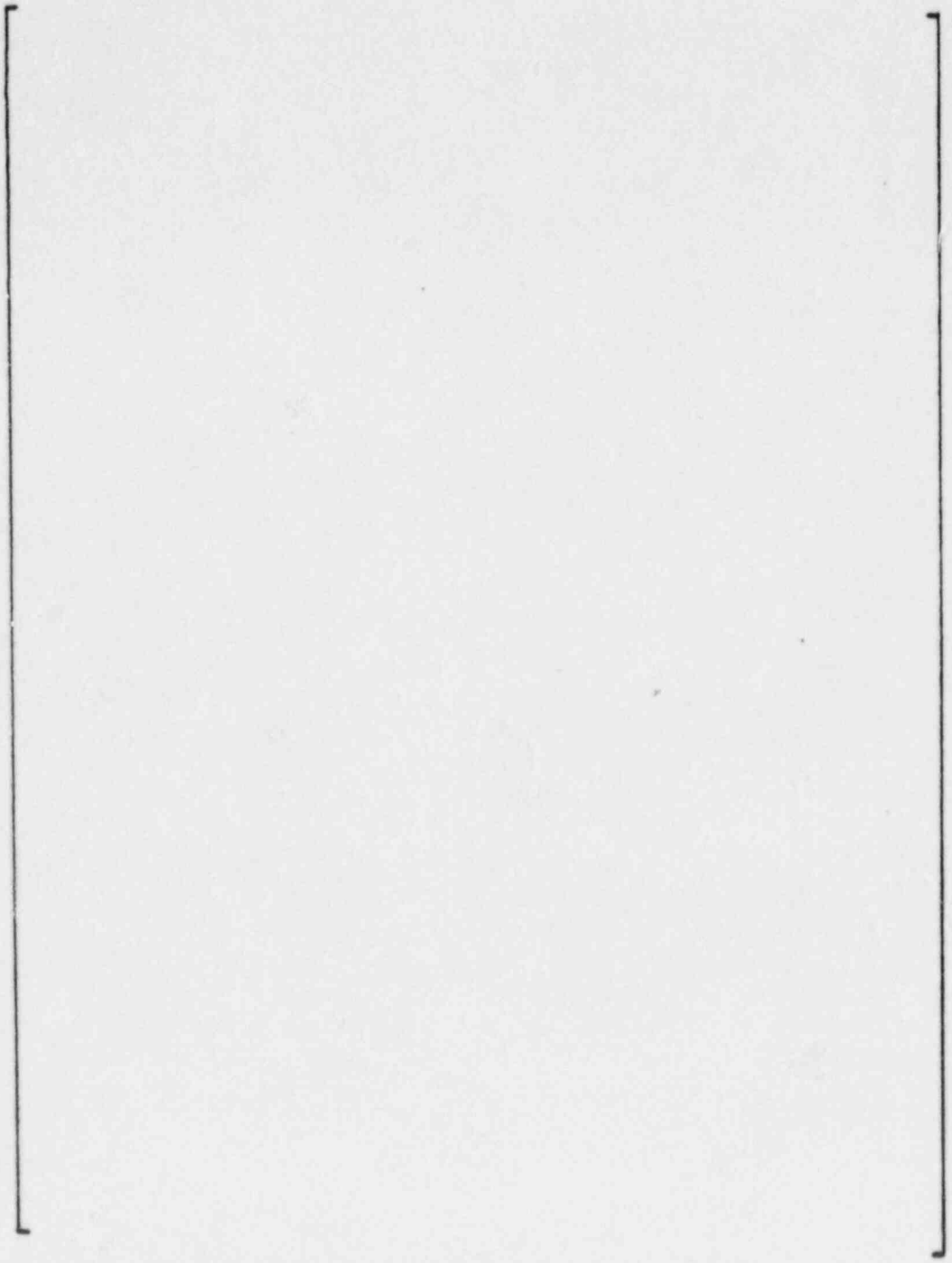

Figure 7-10 Average Velocity and Density in the Plane of the U-Bends Normal to Row 10

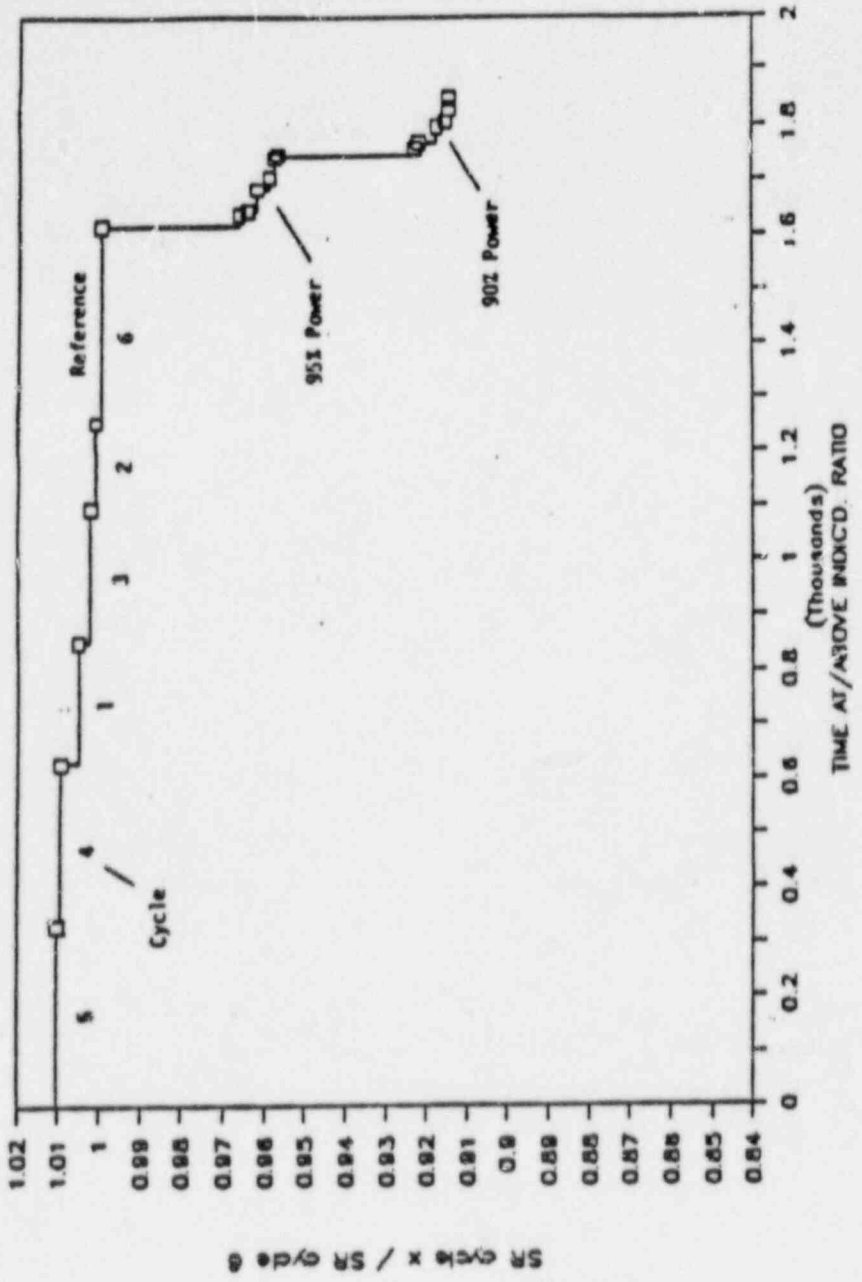

Figure 7-11 Beaver Valley 1 Normalized Stability Ratio Based on High Power (>86%) Operation

8.0 PEAKING FACTOR EVALUATION

This section describes the overall peaking factor evaluation to define the test based peaking factors for use in the tube fatigue evaluation. The evaluation of the eddy current data to define the AVB configuration for North Anna-1 Tube R9C51 is described. This configuration is critical to the tube fatigue assessments as the peaking factors for all other tubes are utilized relative to the R9C51 peaking factor. Uncertainties associated with applying the air model test results to the tube fatigue assessments are also included in this section. Included in the uncertainty evaluation are the following contributions:

- o Extrapolation of air test results to two phase steam-water
- o Cantilever tube simulation of U-bend tubes
- o Test measurements and repeatability
- o AVB insertion depth uncertainty

8.1 North Anna-1 Configuration

8.1.1 Background

The AVB configuration of the ruptured tube in North Anna, R9C51, is the reference case for the tube fatigue evaluations for other plants. In accordance with the NRC Bulletin 88-02, the acceptability of unsupported tubes in steam generators at other plants is based on tube specific analysis relative to the North Anna R9C51 tube, including the relative flow peaking factors. Thus, the support conditions of the R9C51 tube are fundamental to the analyses of other tubes. Because of the importance of the North Anna tube, the support conditions of this tube, which were originally based on "AVB Visible" interpretations of the eddy current test (ECT) data (Figure 8-1), were reevaluated using the [ ]^{a,c} developed since the North Anna event. The [

] ^{a,c} The results of this evaluation are summarized below.

8.1.2 Description of the Method

The basic method utilized was the [ ]a,c in which the AVB position is determined based on [ ]a,c In this study, the [ ]a,c technique was utilized in the [ ]a,c The objective of this application was, with the greatest confidence possible, to establish the positions of the AVBs in an 8 column range around the R9C51 tube in North Anna 1, Steam Generator C.

8.1.3 Data Interpretation

The ECT traces for the U-bends in Rows 8-12 (in one case, 13) were examined for Columns 48-55. The original AVB visible calls are shown in Figure 8-1. The data were examined by an eddy current analyst experienced in reading these traces, and by a design engineer knowledgeable in the geometry of the Model 51 U-bend region.

The intent of this review was to determine if the presence or absence of AVBs as shown in Figure 8-1 could be confirmed using the AVB [ ]a,c technique. Preliminary [

]a,c

[

]a,c

Figure 8-4 is the "AVB visible" map for columns 48 through 55, based on the critical review of the data. It should be noted that the original data interpretations and the review interpretations are consistent.

8.1.4 [ ]a,c

[

]a,c

[

]a,c

The logic in arranging the [ ]a,c data is based on the following two rules:

Rule 1. The [ ]a,c of the same AVB based on different tubes in the same column must be consistent.

[

]a,c

Rule 2. Two adjacent tubes in the same row [ ]a,c Consequently, the difference in the [

]a,c

The implementation of this is that if the position (either left or right) of a [ ]^{a,c} AVB is assumed for a column, then the [ ]^{a,c} in the adjacent columns are also [ ]^{a,c}

The arrangement of the AVBs as shown in Figure 8-5 satisfies the rules above and is consistent with the rupture of R9C51. The resulting AVB arrangements, based on the projection matrix of Figure 8-5 is shown in Figure 8-6.

8.1.5 Conclusions

The general AVB arrangement surrounding the ruptured tube in North Anna-1, Steam Generator C, which was the basis for the analysis, is confirmed by a detailed critical review of the ECT data. Differences exist in the AVB pattern between tube columns 48-49, in which the AVBs appear to be less inserted than previously indicated. The pattern of Figure 8-6 is the best fit to the rules which were adopted for determining the position of the AVBs, as well as consistent with explanation of the tube failure.

The basis of the review was a [ ]^{a,c} technique which utilizes [ ]^{a,c} The intent of the review was to establish the positions of the AVBs by confirming or eliminating features of AVB alignments such as side to side offsets, etc. of the AVBs adjacent to the tubes. Overall, the conclusions regarding the positions of the AVBs around R9C51 in North Anna-1, Steam Generator C are based on consistency among all the available data.

8.2 Test Measurement Uncertainties

The descriptions of the peaking factor tests and apparatus were provided in Section 5.4. All practical measures were taken to reduce uncertainties. Nevertheless, some still remain and should be properly accounted for. The important parameter measured during testing that has a significant impact on

peaking factor is the air velocity. The air velocity at test section inlet was measured using a [ ] Based on considerable experience with the use of such instruments, it is known that the magnitude of uncertainty is very small. A [ ] measurement uncertainty is used in this analysis based on past experience.

8.3 Test Repeatability

During the peaking factor testing of AVB configuration, each test was performed at least two times to confirm repeatability. It has been demonstrated that the tests are quite repeatable with the results often falling within 2 or 3% of one another for the repeat tests. An upper bound value of 5% was used in the current uncertainty analysis.

8.4 Cantilever vs U-Tube

A first order estimate can be made of the validity of modeling a U-bend tube by a cantilever tube in tests to determine the effects of AVB insertion depth on the initiation of fluidelastic vibration. The following assumptions are used:

1. [

2.

3.

] a,c

4. [

]a,c

For the purposes of this estimate, the geometry of the cantilever measuring tube in the air test model is compared with the geometry of a prototypical Row 10 tube. [

]a,c

The comparison between a U-bend tube and the model tube involve the consideration of an effective velocity associated with the flow perturbation caused by the AVBs. [

]a,c

[

]^{a,c} Using these values, the ratio of the effective velocity for the cantilever measuring tube to that for the U-bend tube is about [ ]^{a,c} for the case treated.

A similar evaluation can be made for a Row 10 tube that lies in the projection or shadow of an AVB that is inserted to a dept required to support a Row 9 tube. [

]^{a,c} The net result is that the ratio of the effective velocity for the cantilever tube to that for the U-bend tube is about [ ]^{a,c}

These results indicate that, for the particular assumptions used, the cantilever tube model appears to be a reasonable representation of the U-bend with respect to determining relative peaking factors for different AVB configurations. This evaluation also shows that, on the average, the magnitude of the systematic uncertainty associated with the use of cantilever tube to simulate the U-bend is about [ ]^{a,c}

8.5 Air vs Steam-Water Mixture

The local peaking factors from the air tests can be applied tc the steam generator steam/water conditions either as a direct factor on the mixture

velocity and thus a direct factor on a stability ratio, or as a factor on the steam velocity only with associated impacts on density, void fraction and damping. This method leads to a reduction in tube damping which enhances the peaking factor compared to the direct air test value. For estimating an absolute stability ratio, this application of the peaking factor is a best estimate approach. However, for the evaluation of tubes relative to stability ratio criteria, it is more conservative to minimize the peaking factor for the North Anna Unit 1 tube R9C51 through direct application of the air test peaking factor. This conservative approach is therefore used for evaluating tube acceptability.

Under uniform AVB insertion (or aligned AVB insertion), there are no local open channels for flow to escape preferentially. Therefore, air flow is approximately the same as steam/water flow relative to velocity perturbations. Under non-uniform AVB insertion the steam/water flow may differ from air, as the steam and water may separate from each other when an obstruction, such as an AVB, appears downstream. The water would continue along the same channel while steam readily seeks a low resistance passage and thus turns into adjacent open channels. Two phase tests indicate a tendency for steam to preferentially follow the low pressure drop path compared to the water phase.

Based on the above discussion, the F_i are considered to more appropriately apply to the steam phase. Thus, it follows that mixture mass velocity for the tube subject to flow perturbation can be written as follows:

[ ]a,c

where D_g is the vapor density, D_f the water density, F_a the velocity peaking factor determined from air tests, j_g^* the nominal superficial vapor velocity, and j_f^* the superficial water velocity. Steam quality can then be determined as follows:

[ ]a,c

The [ ]a,c as used in the ATHOS code, is applied to determine void fraction. Subsequently, mixture density, velocity and damping coefficients for the tube which is not supported and subject to flow perturbation is evaluated. Therefore, similar to the air velocity peaking factor, local scaling factors of mixture density and velocity and damping coefficient can be readily determined. Finally, a local stability peaking factor for fluidelastic vibration can be calculated as follows:

[ ]a,c

where F_s is the stability peaking factor, F_d the density scaling factor, F_v the velocity scaling factor, and F_{dp} the damping coefficient scaling factor. If we use the air velocity peaking factor without translating to steam/water conditions, then

[ ]a,c

As shown in Table 8-1 stability peaking factors for the steam/water mixture are slightly higher than air velocity peaking factors. The difference between the steam/water and air peaking factors increases as the air peaking factor increases.

For application to tube fatigue evaluations, the ratio of the peaking factor for a specific tube to that for North Anna R9C51 is the quantity of interest. Larger values for this ratio are conservative for the tube fatigue assessment. The North Anna R9C51 peaking factor is one of the highest peaking factors. As discussed in Section 8.7, a peaking factor of nearly [ ]a,c is determined for the R9C51 tube. The differences between [ ]a,c Typical values are shown in Table 8-2. These results show that the direct

application of the air test data yields the higher relative peaking factor compared to R9C51. To obtain conservatism in the peaking factor evaluation, the[ ]^{a,c}

Comparing the values in the first and last columns of Table 8-1, it may be noted that the stability peaking factor for steam water is[ ]^{a,c}higher than the air velocity peaking factor. On the average, the uncertainty associated with the conservative use of air velocity peaking factor is[ ]^{a,c}

The conclusion that peaking factor for steam water flow would be higher due to the dependency of damping ratio on void fraction was supported by an alternate study. In this study, a section of steam generator tubes were simulated using the ATHOS code under protypic flow conditions. The objective of this study was to examine the magnitude of the changes in void fraction and thus stability ratio as a consequence of non-uniform AVB insertion patterns. The current version of ATHOS has modeling limitations that prevent accurate modeling of local geometry effects. In addition, it is believed that an analysis using two-fluid modeling procedure is mandatory to a calculation of the peaking factors for a steam generator to account for the preferential steam flow along the low resistance path. Consequently, the intent of this analysis is only to help bound the uncertainty on void fraction effects from extrapolating the air tests to steam-water.

First the analysis was conducted with uniformly inserted AVB's in the ATHOS model. The ATHOS results were processed by the FLOVIB code to determine stability ratios for the specific tubes of interest. The calculation was repeated using a non-uniform AVB insertion pattern in the model. The results show that the void fraction distribution changes as a result of flow perturbation. Further, the impact on stability ratio resulting from the changes in void fraction profiles was about[ ]^{a,c}This alternate calculation provides independent corroboration of the prior discussion regarding the stability peaking factors under steam-water conditions vs in air.

8.6 AVB Insertion Depth Uncertainty

The most significant uncertainty for the low peaking configurations is not in the test results, but in the determination of actual AVB insertion patterns adjacent to specific tubes. The methodology used for obtaining the AVB insertion patterns from eddy current data can ascertain the AVB location only to within approximately [ ]a,c
The effect on peaking factor resulting from this uncertainty is addressed using test results of AVB configurations that varied from one another by up to [ ]a,c

Based on maps of AVB insertion depth of various plants, several configurations have been tested for determining fluidelastic instability flow rate by an air cantilever model. Stability peaking factors were then determined from the ratio of critical flow rate for a uniform AVB insertion configuration to a specific configuration. Figure 8-7 summarizes the AVB configurations tested.

Position of AVB insertion depth is determined from Eddy Current Test (ECT) data. Positioning of AVB from ECT data reading is subject to uncertainty; its accuracy is probably about [ ]a,c A change of an AVB insertion depth in a given configuration leads to a different configuration, and thus a different peaking factor. A review of the tested AVB type has been made and results summarized in Table 8-3. As can be seen, a decrease in depth of an appropriate AVB tends to decrease the peaking factor, for instance, a [ ]a,c Such a trend can be explained; a decrease in a specific AVB depth will open up more channels for incoming fluid to distribute and thus less flow perturbation. However, this applies only to those changes without inducing the reinforcement of flow perturbation from upstream to downstream.

On the average, the uncertainty in peaking factor resulting from small variations in AVB insertion (of the order of 1/2 tube pitch) is found to be [ ]a,c

8.7 Overall Peaking Factor with Uncertainty

As discussed in the previous subsections, there are several aspects to be considered in applying the laboratory test data to steam generator conditions. These considerations were reviewed one at a time in those subsections. This section will integrate the pieces into one set of stability peaking factors.

Looking forward to how these peaking factors are used in the analysis (Section 9), the relative stability ratio calculated for a given tube without the consideration of flow peaking is corrected using the ratio of the peaking factor of the specific tube to that of the North Anna R9C51 tube (Configuration 1a). It is to be noted that, of all the configurations tested, configuration 1b produced the highest peaking factor, followed very closely by 4c, 1a and 5e. This is encouraging in the sense that it tends to explain why, of all the tubes in service, the R9C51 tube was the one to experience the fatigue rupture.

It is to be noted that the test results would be applied as ratios of a specific tube peaking factor to the R9C51 peaking factor. This will reduce the influence of some uncertainties since the systematic uncertainties would affect both the numerator and the denominator in the ratio of peaking factors. The major difference will be in those configurations whose peaking factors are significantly lower than that of R9C51. The approach employed here is intended to provide that conservative peaking factors are employed for such apparently low peaking configurations.

The uniform AVB configuration (2a) is selected as a reference configuration, and the peaking factors of all configurations tested are recomputed on the basis of this reference. As discussed below, some of the test uncertainties are applied to the reference case to account for its significantly low peaking relative to the R9C51 configuration.

The uncertainties in the test results and their extrapolation are those due to test measurements, test repeatability, cantilever tubes in the test vs U-tubes in the steam generator, and air tests vs steam-water mixture. These

were discussed in more detail in the previous subsections. The magnitude of these uncertainties are listed in Table 8-4.

Of these uncertainties, those due to measurement and repeatability of tests are random errors and can occur in any test. Therefore, these are treated together. The total random uncertainties are calculated by [ ]^{a,c} The RSS value of these is [ ]^{a,c} Since these can occur in any test, these are to be applied to all tests. One way of doing this is to apply it to the R9C51 value, that being in the denominator of the final peaking factor ratio. Thus the peaking factor for configuration 1a (R9C51) is reduced by this amount to yield a value of [ ]^{a,c} instead of the [ ]^{a,c} appearing in Table 5-2.

The next three uncertainties in Table 8-3 are systematic uncertainties. It could be argued that these appear in the peaking factors of both the specific tube under consideration and the R9C51 tube and are therefore counter balanced. However, the relative magnitude of these may be different, particularly for configurations with much lower peaking than R9C51. Therefore it was judged that the [ ]^{a,c} Similarly, as noted above, the effect on peaking factor due to the uncertainty in the field AVB configuration is also included in this reference case. Thus, [ ]^{a,c} The peaking factor of the reference configuration 2a (Table 8-5) is raised by his amount to a value of [ ]^{a,c}

The change in peaking factors of configurations 1a and 2a resulting from the application of uncertainties as described above are shown in Column 3 of Table 8-4. The peaking factors of all configurations are recomputed on the basis of this reference configuration (2a). These values are displayed in Column 4 of Table 8-4.

Some of the uncertainties were applied to the reference configuration (2a) in order to apply them to all low peaking configurations conservatively. Thus, no configuration should have a lower peaking factor than this reference configuration. Therefore, when a peaking factor value less than [ ]^{a,c} is calculated for any configuration, (in Column 4 of Table 8-5), it should be altered to [ ]^{a,c} Further, for some of the configurations that are conceptually similar, the more limiting (higher) value is used. For example, a peaking factor of [ ]^{a,c} is used for configurations 5a and 5b based on their similarity to configuration 5c.

The final stability ratio peaking factors calculated on this basis (with configuration 2a as the reference) are shown in Table 8-6. It may be noted that the peaking factors vary in the range [ ]^{a,c} the R9C51 peaking factor being [ ]^{a,b,c} Figure 8-7 shows the final peaking factors with the pictorial representation of the AVB insertion patterns.

Table 8-7 shows the result of applying the peaking factors to specific tubes in the Beaver Valley Unit 1 steam generators.

The overall conclusions from the peaking factor assessment are:

1. As noted in Table 8-4, five elements have been included in the uncertainty evaluation for the peaking factors. The uncertainty estimates were developed from both test and analysis results as described in Sections 8.2 to 8.6. The largest single uncertainty of [ ]^{a,c} is attributable to uncertainties of up to [ ]^{a,c} on determination of AVB insertion depths from field eddy current data. This relatively large uncertainty is applicable only to low peaking conditions where the AVB uncertainties can contribute to small peaking factors. The definition of "no flow peaking" was increased to encompass the small peaking effects from AVB insertion uncertainties. For the AVB patterns leading to significant peaking factors, AVB's were positioned within uncertainties to maximize the peaking factor. For these configurations, variations of AVB insertion within these uncertainties are expected to reduce the peaking factor compared to the final values of Table 8-6 and Figure 8-7.

2. Including uncertainties directed toward conservatively decreasing the peaking factor for the North Anna tube R9C51, the final R9C51 peaking factor is [ ]^{a,b,c} relative to a no flow peaking condition such as with uniform AVB insertion depths.

3. The final peaking factors include peaking effects greater than the R9C51 tube (such as configuration 4c) although this is believed to be a consequence of the conservative uncertainty analysis and is not likely to be representative of actual peaking effects.

Table 8-1

Stability Peaking Factor Due to Local Velocity Perturbation

Scaling Factors for Steam/Water

Air Velocity Peaking Factor, F_a	Void Fraction Scaling, F_v	Density Scaling, F_d	Velocity Scaling, F_v	Damping Scaling, F_{dp}	Stability Peaking Factor, F_s
[					]^{a,c}

NOTE: 1. Stability peaking factor for steam/water mixture is calculated as follows:

[ ]^{a,c}

2. Damping scaling factor is calculated using modal effective void fraction of [ ]^{a,c} for R9C51 tube.

Table 8-2

Comparison of Air and Steam-water Peaking Factor Ratios

Air Peaking Factor	Air Peaking Ratio	Steam Peaking Factor	Steam Peaking Ratio
[			]a,c

Table 8-3

Effect of Local Variation of AVB Insertion

Type A	Type B	A to B AVB Variation	Peaking Factor A	Peaking Factor B	Ratio (B/A)
5b	5a	[			]a,c
4a	5c				
5c	5a				
5a	5b	[			]a,c
5c	4a				
5a	5c				

Table 8-4

Uncertainties in Test Data and Extrapolation

	Source of Uncertainty	Type	Magnitude, %
1.	Velocity measurement	Random	[ ] a,c
2.	Test repeatability	Random	
3.	Cantilever vs U-tube	Systematic	
4.	Air vs steam-water mixture	Systematic	
5.	Field AVB configuration	*	

* This is not an uncertainty associated with the test data. It results from the inaccuracy in determining the true AVB position in the field using eddy current data.

Table 8-5

Extrapolation of Test Results to Steam Generator Conditions

Configuration	Test Data	Data with Uncertainties	Peaking Factor Referenced to Config. 2a
1a	[		a,b,c]
1b			
2a			
3			
4a			
4b			
4c			
4d			
4f			
5a			
5b			
5c			
6c	]		

Table 8-6

FINAL PEAKING FACTORS

Configuration	Peaking Factor
1a	[a,b,c]
1b	
2a	
3	
4a	
4b	
4c	
4d	
4f	
5a	
5b	
5c	
6c	

Table 8-7

Stability Peaking Factors for Specific Tubes

BEAVER VALLEY UNIT 1

STEAM GENERATOR	ROW NO.	COLUMN NO.	PEAKING FACTOR *
A	8	60	[ ] a,b,c
	8	61	
	9	35	
	10	43	
	ALL OF THE REMAINING		
B	9	35	
	9	60	
	ALL OF THE REMAINING		
C	9	60	
	10	60	
	11	47	
	11	51	
	11	52	
	12	51	
	ALL OF THE REMAINING		

* The peaking factor is divided by 1.47 to obtain the relative flow peaking factor to R9C51 of North Anna 1.

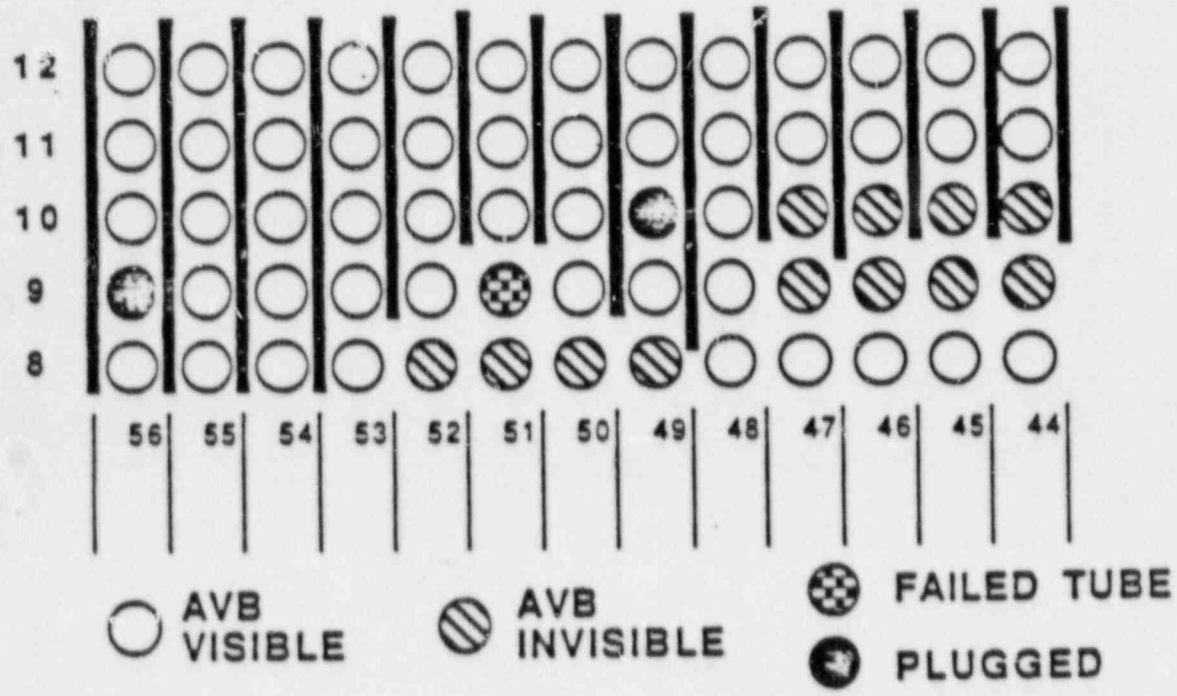

Figure 8-1 Original North Anna AVB Configuration

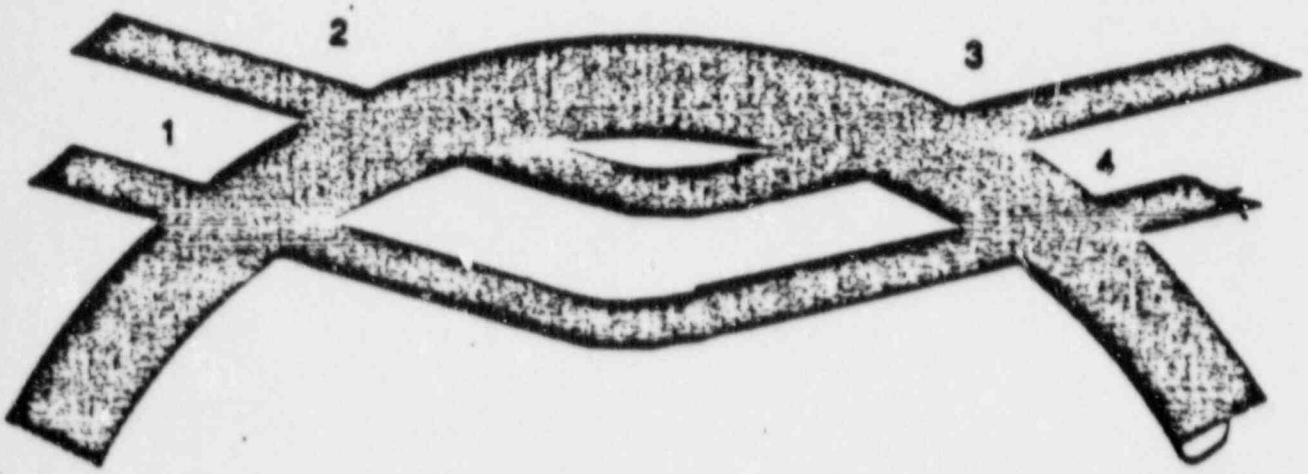

Figure 8-2 Schematic of Staggered AVBs

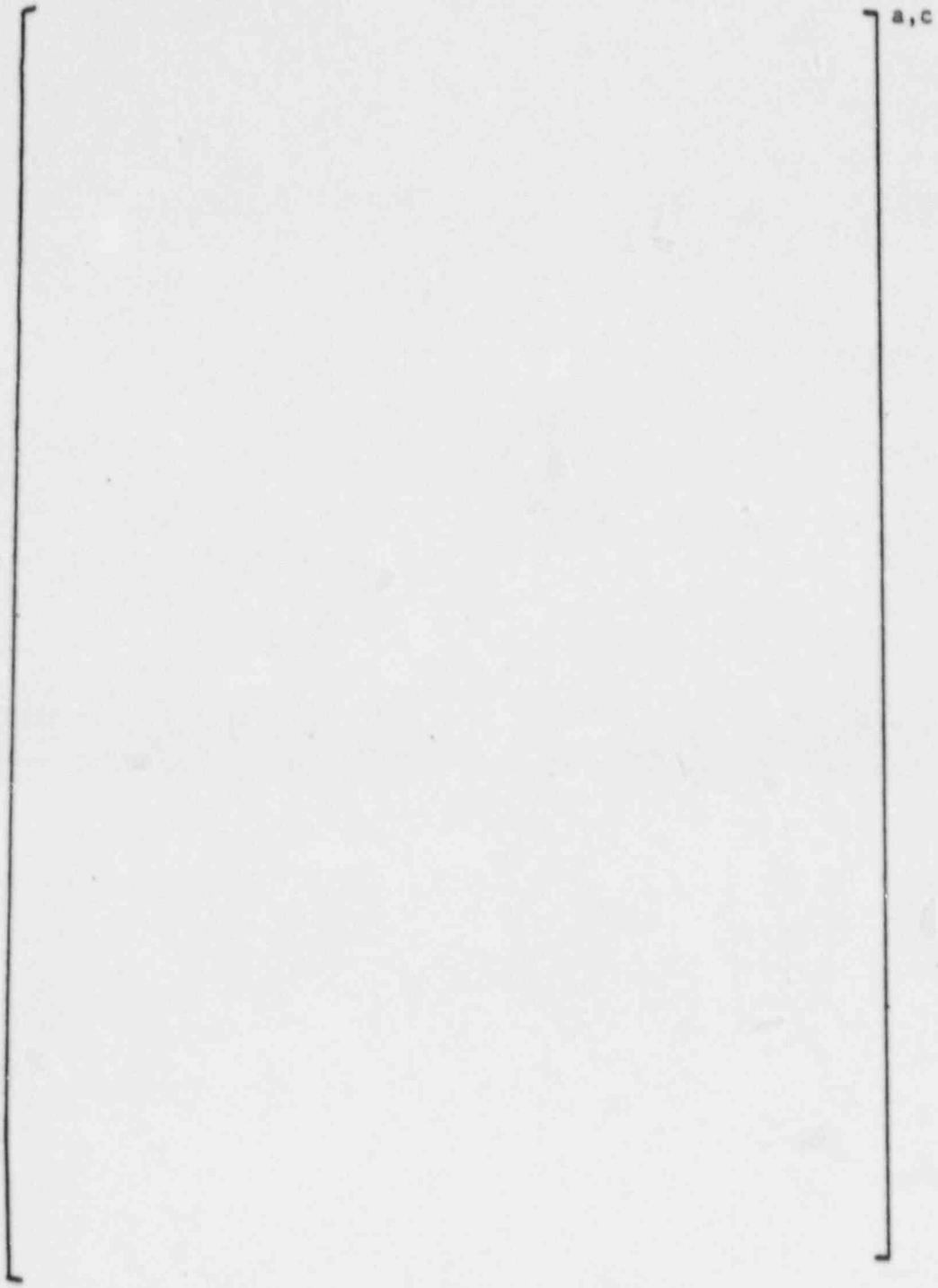

Figure 8-3 AVB "Pair" in ECT Trace

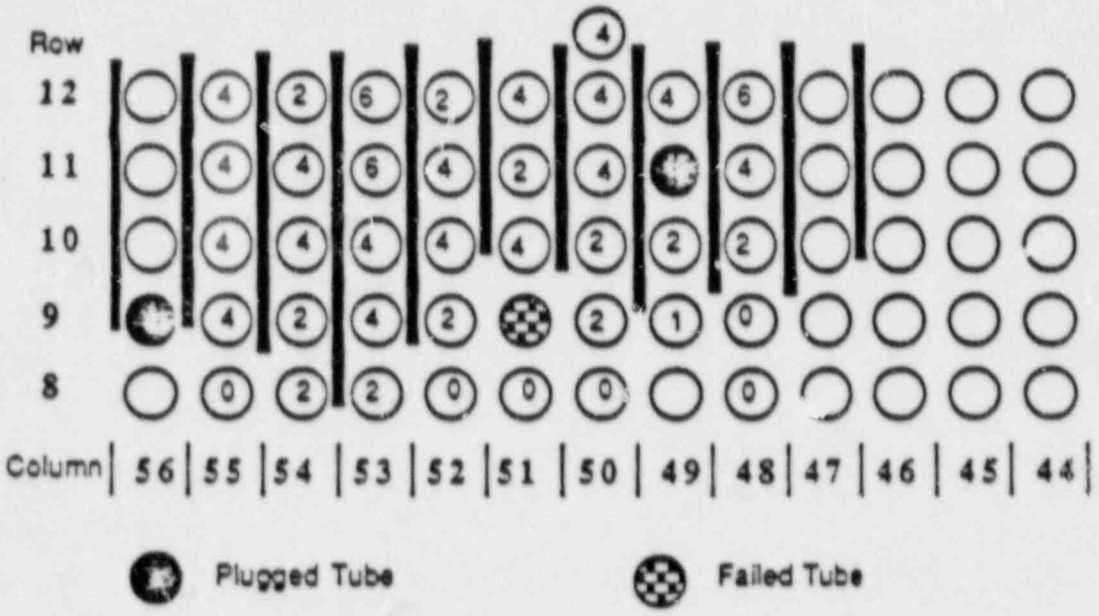

Numbers in circles in column range 48-55 represent readable AVB intersection signals, based on critical review of the ECT traces.. Open circle in this range means no data is available.

Figure 8-4 North Anna 1, Steam Generator C, AVB Positions
Critical Review "AVB Visible" Calls

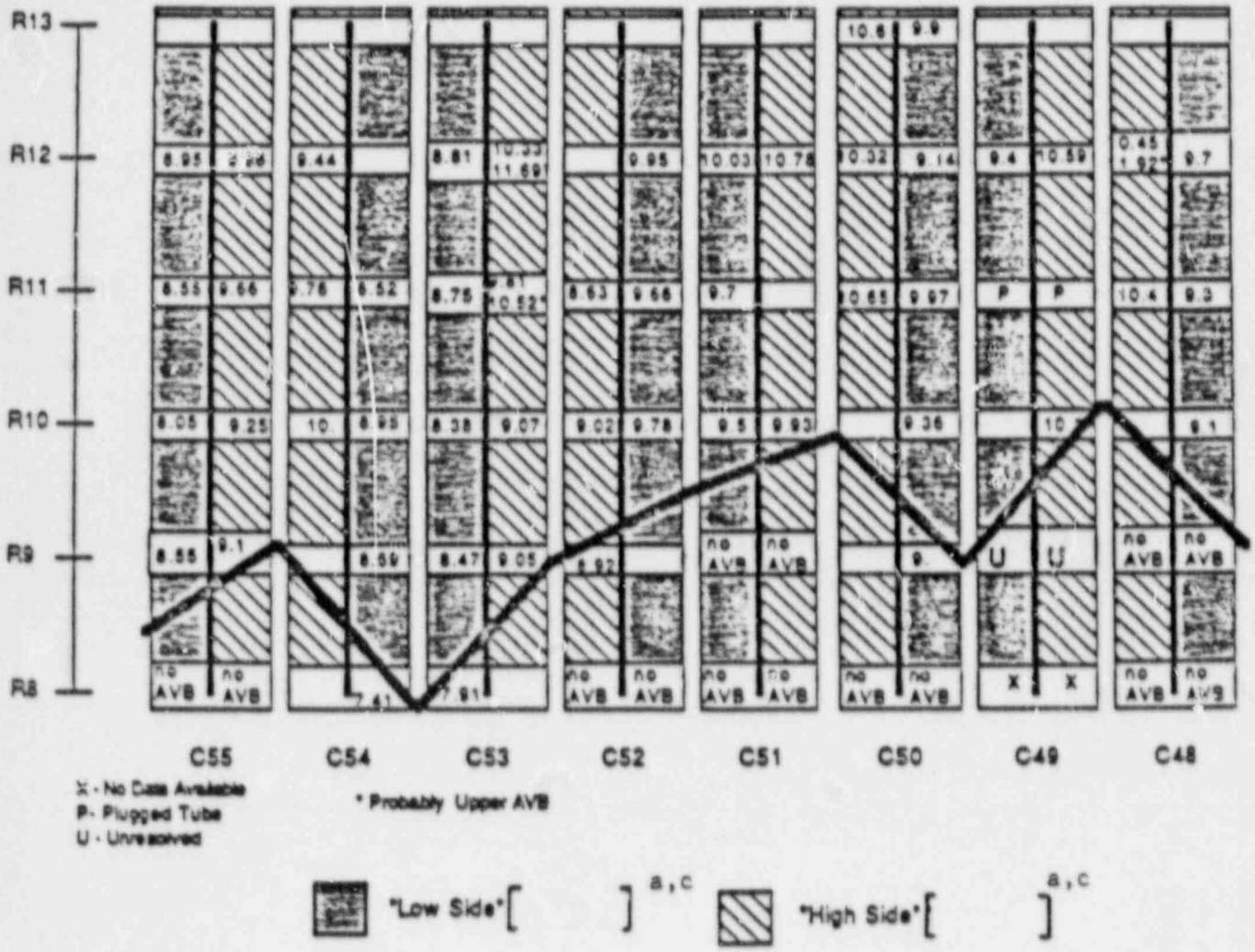

Figure 8-5 North Anna 1, Steam Generator C, R9C51 AVB[ ]a,c Matrix

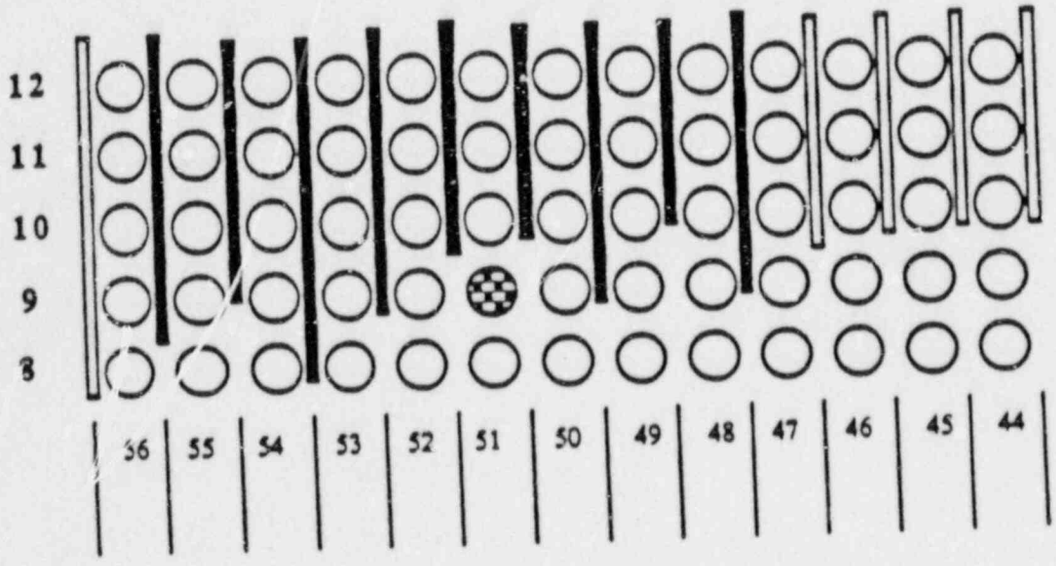

Figure 8-6 North Anna R9C51 AVB Final [ ]a,c Positions

TYPE OF AVB INSERTION	PEAKING FACTOR	TYPE OF AVB INSERTION	PEAKING FACTOR
1a	[a,b,c]	4d	[a,b,c]
1b		4f	
2a		5a	
3		5b	
4a		5c	
4b		6c	
4c			

Figure 8-7 FINAL PEAKING FACTOR FOR BEAVER VALLEY 1

9.0 STRUCTURAL AND TUBE VIBRATION ASSESSMENTS

9.1 Tube Mean Stress

This section summarizes an analysis to determine stresses in a dented tube at 100% power. Loads imposed on the tube correspond to steady-state pressure, differential thermal expansion between the tube and the support plate, and a thru-wall thermal gradient. The analysis assumes the tube to be [ ]^{a,c} at cold shutdown.

A summary of the temperature and pressure parameters at 100% power in the vicinity of the top support plate are provided in Table 9-1. The tube temperature corresponds to the average of the primary-side water temperature and the plate temperature. The resulting tube/plate radial interference is [ ]^{a,c}

The analysis is performed using the finite element model shown in Figure 9-1. The model prescribes [

]^{a,c}

Two reference cases were run using the finite element model, the first for a primary-to-secondary side pressure gradient, and the second for a [ ]^{a,c} radial interference between the tube and plate. The pressure case incorporates the axial load on the tube by applying a pressure loading along the top face of the model. Plots showing the distribution of stress for the tube outer surface for the two reference cases are provided in Figures 9-2 and 9-3. Tube stresses due to the thru-wall thermal gradient are calculated to be 9.8 ksi using conventional analysis techniques. A plot showing the combined stress distribution along the tube length, incorporating appropriate scale factors for the Beaver Valley Unit 1 operation conditions, is provided in Figure 9-4. The maximum axial tensile stress is 23.1 ksi and occurs approximately 0.125 inch above the top surface of the support plate. Adding, for conservatism, the surface stress

due to pressure, 0.75 ksi, gives an applied mean stress of 23.3 ksi. In addition to the applied stress, residual stresses exist in the tube as a result of the manufacturing process. For mill annealed tubes with subsequent straightening and polishing, residual stresses exist in the tube. The stresses are compressive at the tube surface, but 5-10 mils below the surface, the stress levels change to 10-15 ksi tensile, Reference 9-1. Combining the applied and residual stresses results in a cumulative mean stress of 38.9 ksi.

9.2 Stability Ratio Distribution Based Upon ATHOS

An assessment of the potential for tubes to experience fluid elastic instability in the U-bend region was performed for each of the tubes in rows eight through twelve. This was performed using FASTVIB, a Westinghouse proprietary finite element based computer code and PLOTVIB, a post processor to FASTVIB. These codes were written to predict the individual responses of an entire row of steam generator tubing exposed to a tube location dependent fluid velocity and density profile. The program calculates tube natureal frequencies and mode shapes using a linear finite element model of the tube. The fluid elastic stability ratio U_e/U_c (the ratio of the effective velocity to the critical velocity) and the vibration amplitudes caused by turbulence, are calculated for a given velocity/density/void fraction profile and tube support conditin. The velocity, density and void fraction distributions are determined using the ATHOS computer code, as described in Section 7.3. Also input to the code are the WECAN generated mass and stiffness matrices used to represent the tube. (WECAN is also a Westinghouse proprietary computer code.) Additional input to FASTVIB/PLOTVIB consists of tube support conditions, fluid elastic stability constant and turbulence constants.

This process was performed for the Beaver Valley Unit 1 steam generator tubes and also for the North Anna Row 9 Column 51 tube (R9C51) using similarly appropriate ATHOS models. Ratios of the Beaver Valley Unit 1 results to those for North Anna Unit 1 R9C51 were generated to produce a quantity that could be used to provide an initial assessment of the Beaver Valley Unit 1 tubes relative to the ruptured tube at North Anna Unit 1.

Figure 9-5 contains the results of this process for each of the rows under investigation. This figure was generated using the following conditions for both Beaver Valley Unit 1 and North Anna Unit 1:

1) Tube is fixed at top tube support plate.

2) Void fraction dependent damping used.

3) No AVB supports active.

A horizontal line is drawn at the relative stability ratio value of 0.90. This identifies the point where a ten percent reduction in stability ratio exists relative to North Anna R9C51. (See Section 4.1 for a discussion of the stability ratio reduction criteria.) All the tubes with ratios above this line would be considered to have stability ratios larger than ninety percent of North Anna R9C51. This figure indicates that all tubes in Row 8 and 9 can be considered acceptable with some tubes being unacceptable in Row 10. Essentially all inner tubes in Rows 11 and 12 lay above this line. Tubes above this line, that are not supported by AVBs, require further evaluation to determine the acceptability of the tubes. Section 9.3 contains the results of the further evaluation for these tubes.

9.3 Stress Ratio Distribution With Flow Peaking

An evaluation was performed to determine the ratio of the Beaver Valley Unit 1 tube stress over the North Anna R9C51 tube stress. This ratio is determined using relative stability ratios discussed in the previous section, relative flow peaking factors (Table 8-7 factors divided by 1.47) and bending moment factors. Sections 4.2 and 4.3 contain additional information and describe the calculational procedure used to obtain the results presented in this section. The results contained in this section are based upon the following conditions:

1) Tube is fixed in top tube support plate.

2) Damping is void fraction dependent.

3) AVBs do not provide support.

4) 10% criteria with frequency effects used.

5) The tubes are assumed to be dented or undented.

6) Flow peaking factors are used.

A tube can be considered acceptable if the stress ratio is less than 1.0 when calculated using the procedure described in Sections 4.2 and 4.3 and including the conditions listed above. Using this criteria indicates that the stress acting on a given tube will not produce a fatigue event in a manner similar to the rupture that occurred in the R9C51 tube at North Anna Unit 1. Figure 9-6 contains the stress ratio results for each of the Beaver Valley Unit 1 tubes in Rows 8 through 12. This figure is applicable for tubes that are dented (tube deformation) at the top tube support plate. As can be observed in the figure, the tubes in Rows 8 and 9 fall below the acceptance line indicating that the tubes are acceptable with respect to U-bend fatigue. All of the tubes in Row 10, except for Column 35, and all of the tubes in Row 11, except for the Column 43, 44, and 47 also fall below the acceptance line. The tubes in these two rows (10 and 11) that do not lay below the acceptance line have large stress ratios due to the large peaking factors associated with these tubes. Most of the tubes in row 12, except for tubes in column 3, 4 and 34 through 47, also fall below the acceptance line. This indicates that the tubes are not acceptable, with respect to U-bend fatigue, if the tubes are not supported by AVBs and are dented at the top tube support plate.

Figure 9-7 contains results similar to the information presented in the previous figure except that the tube is assumed to be undented, but clamped due to support plate corrosion, at the top tube support plate. The conclusions that can be drawn from this figure are almost identical to the conclusions that can be drawn from the previous figure. This figure indicates that all of the tubes in rows 8 and 9 fall below the acceptance line indicating that the tubes are acceptable with respect to U-bend fatigue. All of the tubes in row 10, except for column 35, and all of the tubes in row 11, except for column 43, 44, and 47 also fall below the acceptance line. The tubes in these two row (10 and 11) that do not lay below the acceptance line have large stress ratios due to

the large peaking factors associated with these tubes. Most of the tubes in row 12, except for tubes in column 3, 4 and 36 through 47, also fall below the acceptance line. This indicates that the tubes are not considered acceptable, with respect to U-bend fatigue, if the tubes are not supported by AVB and are firmly fixed, but not dented, at the top tube support plate.

9.4 Cumulative Fatigue Usage

All tubes that are unsupported and have a stress ratio ≤ 1.0 have a maximum stress amplitude that is < 4.0 ksi (from 9.5 ksi) since a 10% reduction in the stability ratio for the North Anna Row 9 Column 51 tube was the criteria basis. The stability ratios for the Beaver Valley Unit 1 tubing are based on the current operating parameters and with future operation on the same basis, the tubes will not rupture as a result of fatigue if 1) they meet the stress ratio criteria of ≤ 1.0 and 2) their current and future fatigue usage will total less than 1.0.

All tubes in the evaluation have been considered to be dented. Table 9-2 contains a summary of the combined relative stability ratios and the stress ratios for the most critical tubes in each of the steam generators. With the exception of five tubes in Steam Generator C, all tubes have relative stability ratios less than 0.9 and stress ratios less than 1.0. The five tubes exceeding these criteria are R12C51, R11C52, R11C51, R11C47 and R10C60 in Steam Generator C. Six tubes have been plugged as a preventive measure to eliminate them from further consideration. Sentinel, or tell-tale, plugs were used to permit detection of tube degradation if it should occur in the future. One tube in Steam Generator A, R10C43, was plugged based on preliminary results.

Acceptability of the Beaver Valley Unit 1 tubing for fatigue is accomplished by demonstrating the acceptability of the tubes with the highest stress ratio, 0.77, at Row 9 Column 35 and Column 60 of Steam Generator B and Row 9 Column 60 of Steam Generator C. The maximum stress with the current operating conditions is

$$\sigma_a = 0.77\ (4.0) = 3.08 \text{ ksi}$$

Based on the relative stability ratio over the operating history presented in Section 7.5, the alternating stress for each operating cycle can be determined. Computing stress ratios for each cycle establishes the maximum alternating stress for each operating cycle. The number of cycles of vibration is obtained for each fuel cycle by multiplying the number of days times the number of cycles per day at the frequency of the Row 9 tube, [ ]^{a,c} hertz.

Conservatively assuming that all fuel cycles have been at 3.08 ksi, the cumulative fatigue usage for the operating license period (with future operational years at the same operating conditions as cycle 6) would be 0.346. All of the unplugged Beaver Valley Unit 1 tubes, therefore, meet the fatigue usage requirement of 1.0 with denting assumed to exist from initial startup.

Table 9-1

100% Power Operating Parameters
Beaver Valley Unit 1

Primary Pressure	= 2235 psi
Secondary Pressure	= 799 psi
Pressure Gradient	= 4360 psi

Primary Side Temperature	= 576°F
Secondary Side Temperature	= 518°F
Tube Temperature	= 547°F

Table 9-2

Beaver Valley Unit 1 Evaluation of the Salient
Unsupported U-bends

STEAM GENERATOR	TUBE	RELATIVE STABILITY RATIO(1)	STRESS RATIO(1)
A	R9C35	0.73	0.31
	R9C47	0.66	0.18
	R10C43	0.89	0.81
	R10C47	0.77	0.35
	R11C49	0.88	0.64
B	R9C47	0.66	0.18
	R9C60	0.86	0.77
	R9C35	0.86	0.77
C	R9C60	0.86	0.77
	R10C47	0.77	0.35
	R10C60	1.081	>>1.0
	R11C47	1.272	>>1.0
	R11C51	1.454	>>1.0
	R11C52	1.454	>>1.0
	R12C51	>1.12	>>1.0

(1) All ratios are in comparison to R9C51, North Anna 1, Steam Generator C.

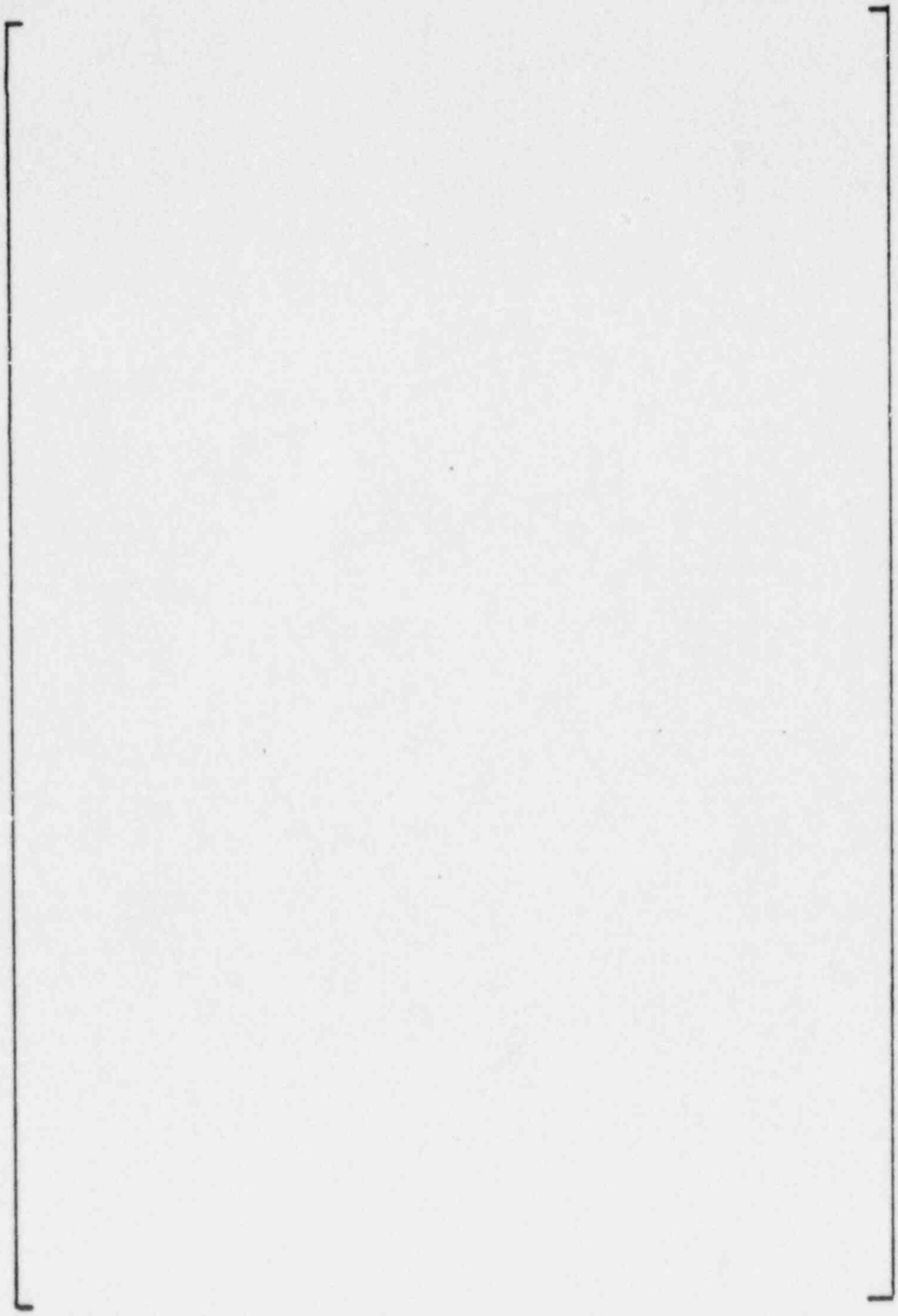

Figure 9-1 Axisymmetric Tube Finite Element Model

[ ] a,c

Figure 9-2 Dented Tube Stress Distributions
Pressure Load on Tube

[

]a,c

Figure 9-3 Dented Tube Stress Distributions
Interference Load on Tube

[ ]a,c

Figure 9-4 Dented Tube Stress Distributions
Combined Stress Results
Beaver Valley Unit 1

[a,c]

Figure 9-5 Relative Stability Ratios Using MEVF Dependent Damping

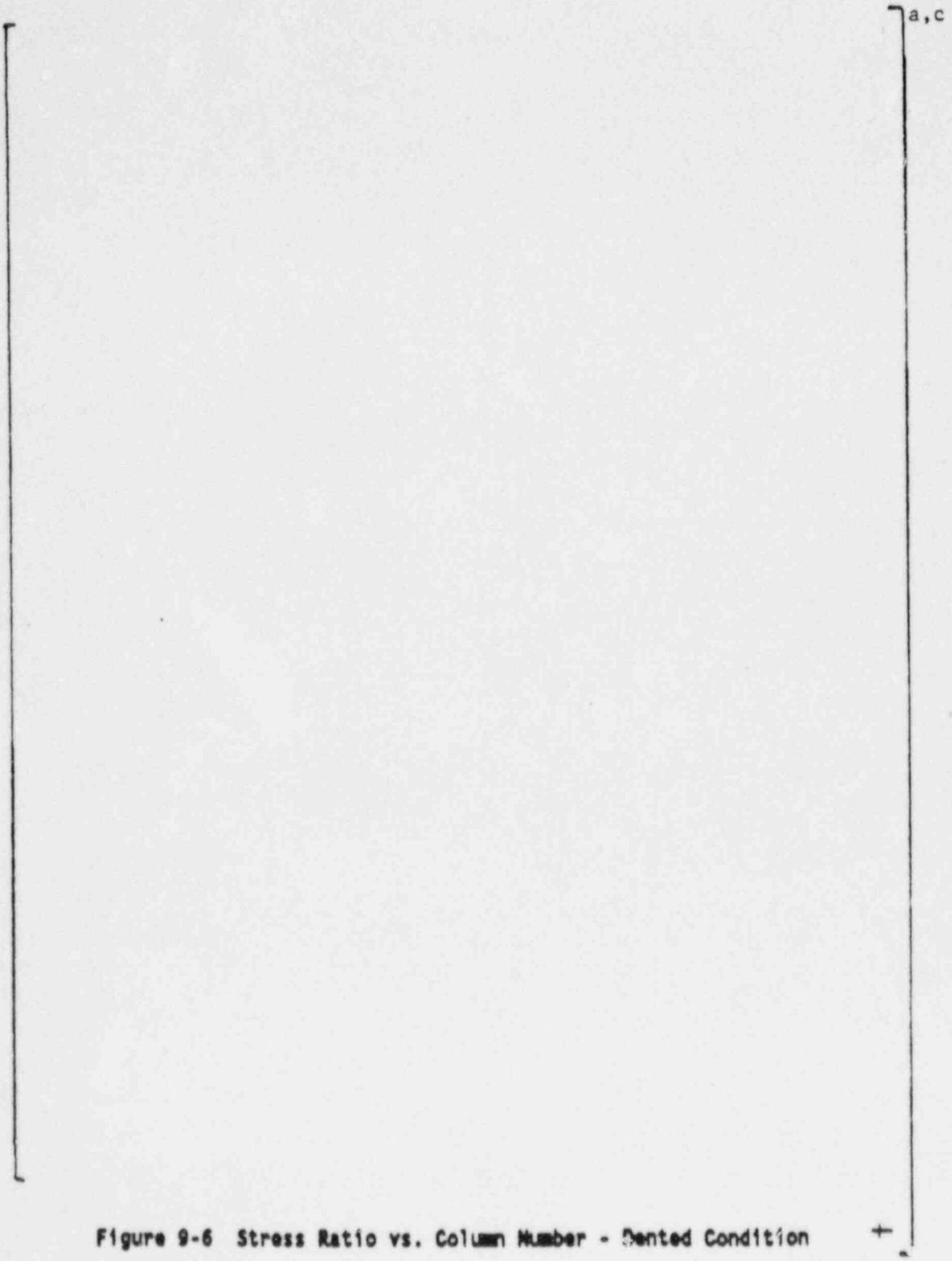

Figure 9-6 Stress Ratio vs. Column Number - Dented Condition

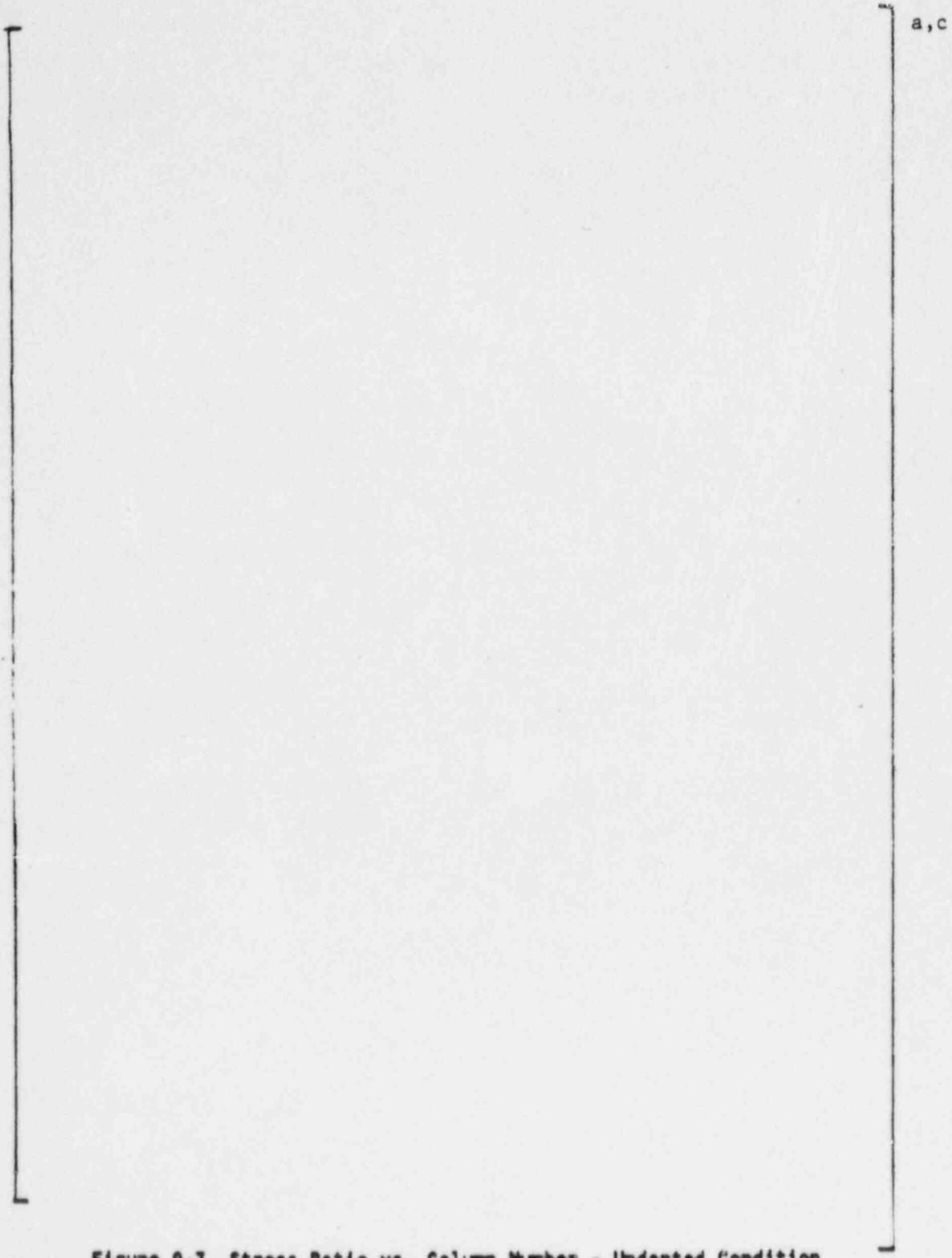

Figure 9-7 Stress Ratio vs. Column Number - Undented Condition